NASA

AMES RESEARCH CENTER

SYSTEM ENGINEERING REPORT (SER) **RB-001**

****

SUBJECT: SOFIA WIND TUNNEL MODEL/STING MODAL ANALYSIS AND MODES MONITORING DURING TEST ENVELOPE CHECK RUN

AUTHOR: RICK BREWSTER

PROJECT : SOFIA

CATEGORY/SUBCATEGORY: TECHNICAL/IN-HOUSE SOFIA-SER

SOURCE: NASA-ARC

DATE: 9/8/92

X-REFERENCE: AIRCRAFT/PRE-DEVELOPMENT

Engineering Memorandum

Subject: SOFIA Wind Tunnel Model/Sting Modal Analysis and Modes Monitoring During Test Envelope Check Run

Date: June 20, 1994

To: Nans Kunz, SOFIA Mechanical Systems Manager, Code EEE

From: Rick Brewster, Sverdrup Technology

I. Introduction

The SOFIA Wind Tunnel Model, in this instance a 2860 lbm, 7% scale model of a Boeing 747-200, is mounted on a 213" sting which is cantilevered from the vertical support strut of the 14' Wind Tunnel. Because of the size of the model and the length of the sting support, the model/sting structure exhibits modal behavior at frequencies lower than normally seen in wind tunnel installations (for this structure on the order of 1 to 3 Hz).

To better understand the model/sting behavior, a modal analysis was performed using a detailed finite element model representation of the support sting and blade. The SOFIA model was represented with a short tube and attached lumped mass. From the finite element analysis a number of system modes were found below 10 Hz, and of these, two major modes were found close to one another around 3 Hz (the first being a lateral rocking and sting torsion resulting in roll of the aircraft model and the second being a vertical sting bending resulting in pitch of the aircraft model). Because of the lowness in frequency and close frequency spacing of these modes, the possibility of a flutter condition of the model/sting system was raised.

Additionally, a lateral divergence analysis using the model/sting finite element model was performed. Lateral divergence was found to be clearly possible, depending on whether conservative air loading assumptions were correct and depending upon the accuracy of the finite element model to predict lateral restoring forces.

The lateral divergence concern was addressed by refining the air load estimates, measuring the sting lateral restoring force, and limiting the lateral travel of the sting.

The flutter concern was addressed by monitoring the modal behavior of the model/sting system during a check run through the planned aircraft model test envelope.

II. Summary

The measured lateral restoring force for the model/sting system was 1568 lbf/degree yaw. The refined model, blade, and sting air load was 674 lbf/degree yaw. The resulting sting divergence criteria was 0.43.

The dynamic response of the model/sting system to the tunnel air stream was monitored throughout a check run where the Mach number and angle of attack settings were varied through the maximum values intended for the aircraft model test (Nm max = 0.88, alpha max = 5 degrees). From power spectrum analysis of aircraft model acceleration measurements, model/sting resonance amplitudes, frequencies, and damping were tracked for frequencies up to 32.5 Hz. Growth in resonance amplitudes were moderate with increasing Mach number and angle of attack setting, and no sharp amplitude increases, common with the onset of flutter, were observed. Resonance peak frequencies did move with changed Mach number, and the frequencies of the two primary modes of concern did cross one another during the run when the lift load compensation system was not used. Modal damping did appear reduced at some higher Mach points, but it appeared not to progressively reduce and was not so close to zero as would be required for the onset of flutter.

Visual observations of the model by the tunnel test personnel were consistent with the power spectrum analysis. No erratic or unstable behavior was observed, and the model obviously did not diverge or flutter, but the low frequency, visually observable modes were judged by some to be less damped at higher Mach numbers.

III. Discussion

A. Finite Element Model

A finite element model representing the sting, blade and aircraft model was created primarily to understand the modal behavior of the model and support system. The overall model is shown in Figure 1. The sting and blade of the model support were modeled in detail with plate and solid elements so to accurately capture the bending and torsional stiffnesses. The aircraft was simply modeled with a short section of tube (of roughly the diameter of the fuselage) extending over the length of the model/blade connection and aft to the estimated mass center of the aircraft model, where a mass lump including estimated inertias was rigidly connected. A bar element with a lumped mass apparent only in the vertical direction was used to represent the counterweight and cable. Bar elements were also used to represent the side tether cables to the sting end. Both the counterweight cable and tether cable bar elements had axial stiffness only and were of the length of the cables themselves. The tether cable elements were pinned to earth at the ends where they attached to the hydraulic damping cylinders, and the counterweight end of the counterweight element was constrained to travel in the vertical direction only. No representation of the lift load compensation system was included. The tether damping system hydraulics were not included other than to assume that for modal analysis they effectively acted as a ground for the tether cable ends. The sting end was fixed to earth and no representation of the tunnel vertical strut was included. See Figure 2 for a solid shaded plot of the sting, blade, and short tube representation of the aircraft model.

B. Modal Analysis

Modal analyses were performed on the model for two cases, one with the lateral tethers attached and one with the tethers unattached. The results of the analysis with tethers attached are shown in Figures 3 through 12 where the first eight modes are plotted. Figure 3 show mode 1 at 3.00 Hz which is a vertical bending of the sting which results in a pitching motion of the aircraft model. Figures 4 and 5 show mode 2 at 3.03 Hz which is a lateral bending/rocking and sting torsion which results in rolling motion of the aircraft model. Figure 6 shows mode 3 at 5.56 Hz which is movement of the counterweight counter to the sting upon the

counterweight cable. Figure 7 shows mode 4 at 6.45 Hz which is a second order lateral bending. Figure 8 and 9 shows mode 5 at 9.15 Hz which is lateral rocking/bending and sting torsion but with the model moving laterally in the opposite direction to the sting. Figure 10 shows mode 6 at 9.98 Hz which is a second order vertical bending. Figure 11 shows mode 7 at 20.96 Hz which is third order lateral bending, and Figure 12 shows mode 8 at 32.38 Hz which is vertical bending where the aircraft model is out-of-phase with the sting.

The modes for the no-tether case are similar to those for the with-tether case except for the low frequency lateral modes. With no tethers the first mode is a lateral bending mode with little torsion and occurs at 1.26 Hz. See Figure 13 for this mode. The second mode is vertical bending at 3.00 Hz as seen in the with-tether case. The third mode of this case is a lateral bending with out-of-phase torsion at 5.06 Hz. See Figure 14 for a plot of this mode. The fourth mode is counterweight plunging as seen in the with-tether case and again is at 5.56 Hz. The fifth mode of the no-tether case appears like a second order lateral bending with model rocking/sting torsion in the direction opposite to sting travel. See Figure 15. All subsequent modes calculated are similar in mode shape and frequency to the with-tether case.

In reviewing the two modal analysis cases, the tethers appear to cause the 1st, 3rd, and 5th modes of the no-tether case (Figures 13, 14, and 15) to convolute to form the 2nd, 4th, and 5th modes of the with-tether case (Figures 4, 7, and 8). Since the damping system hydraulics were assumed to provide a pinned constraint to the tether cable ends, the 1.26 Hz no-tether lateral mode (having little torsion) effectively disappears and the 3.03 Hz with-tether lateral/torsion mode appears in its place. This assumption of the damping system's constraint behavior seems reasonable in light of subsequent testing.

A simple measurement of the low frequency modes was performed by hand exciting the model/sting structure and counting the oscillations over a period of time. For the with-tethers case, the vertical bending mode was measured to be 2.86 Hz and the lateral rocking mode was at 3.20 Hz, which compare to the analysis predicted values of 3.00 and 3.03 Hz respectively. The lateral bending mode in the no-tethers case was measured to be 1.04 Hz which compares to the analysis prediction of 1.26 Hz.

C. Divergence Analysis

The divergence of the sting, i.e. the change in air load per degree of angle change (relative to the airstream) divided by the change in structural restoring force per degree of angle change, was calculated. The final best estimate of the combined model, blade, and sting air loads was 674 lbf/degree of yaw. The structural restoring force was calculated to be 1568 lbf/degree of yaw. The resulting divergence criteria was 674/1568 or 0.43 compared to a commonly accepted maximum divergence criteria of 0.5.

The air load estimate was a result of detailed air loads models generated by Ian Gilchrist of AMI. The structural restoring force value was a result of a lateral stiffness measurement of the sting. Measured lateral translational stiffness was converted to an estimated lateral end rotation stiffness by utilizing the sting stiffness distribution from the sting finite element model.

Sting divergence in the vertical direction had been previously calculated in the sting/model design static analyses to be 0.27. The vertical structural restoring force value calculated in that analysis was corroborated with the finite element model, and no analysis refinement of the air loads was necessary.

D. Flutter Concerns and Monitoring

The existence of relatively low frequency resonance modes of the sting/model structure and the closeness of frequency spacing of these modes raised the concern that a flutter type behavior might occur. One common type of flutter is associated with wings where the torsion mode and bending mode of the wing undergo a merging of frequencies and loss of damping due to the aerodynamic interaction of the wing structure and airstream. The combined torsion and bending oscillation of the wing effectively extracts energy from the airstream which overcomes the energy losses associated with structural and viscous damping, and at a critical airstream velocity the resulting effective damping in the system goes to zero. From that point energy added into the system causes the oscillatory amplitudes to diverge and flutter results. (For a discussion of flutter phenomenon, see Y.C. Fung, The Theory of Aeroelasticity).

The airstream/wing oscillation condition where the wing begins to effectively extract energy from the airstream is known as the point of aerodynamic instability. The energy extracted from the airstream must be absorbed by the energy dissipating capabilities of the structure. This air velocity regime where energy begins to be extracted and absorbed by the system's inherent damping mechanisms exhibits itself as a loss in the measured apparent overall damping of the structure.

Predicting if and when structures will reach an aerodynamic instability condition requires an involved aeroelasticity analysis based on structure air loading and modal characteristics. One simple estimate given by Küssner (see Fung, p. 164) for determining the critical airflow flutter speed for wings is:

$$Ucr = w\,c\,/\,2\,kcr$$

where Ucr is the critical flutter speed in ft/s, w is the torsional frequency of the wing in radians/sec, c is the chord length of the vibrating portion of wing in feet, and kcr is a recommended reduced frequency (or Strouhal number) equal to 0.9 plus or minus 0.12. Solving for w ;

$$w = 2\,Ucr\,kcr\,/\,c$$

For Ucr = 0.88 Nm = 959.2 ft/s (maximum intended tunnel speed),
c = 2.76 feet (estimated from the aircraft model), and
kcr = 0.9 - 0.12 = 0.78 (best case assumption),

then w = 542.2 rad/s = 86.3 Hz or greater to avoid flutter.

No analysis of the aircraft model was performed to determine wing torsion, but rationalizing that wing torsion effectively occurs during vertical bending of the sting, then wing torsion would occur at around 3.00 Hz due to the first with-tethers mode and at 32.38 Hz for the eighth with-tethers mode, far below the best case suggested value of 86.3 Hz.

Though the aircraft model wings were not expected to flutter themselves, the possibility that the model/sting system might exhibit a divergent oscillatory behavior akin to wing flutter, driven by the same wing aerodynamic loads as wing flutter, was considered real and deserving attention. Because flutter often gives little visual

warning of its onset, it was felt that the standard procedure for tunnel model monitoring, i.e. tunnel operator visual and strain gage monitoring, should be augmented with a power spectrum analysis of the model/sting response to tunnel airstream loading.

E. Sting/Model Acceleration Measurements and Power Spectrum Analysis

To monitor the response of the model/sting during tunnel operation, several accelerometers were placed on the structure to measure the lateral and vertical accelerations, and these measurements were analyzed and monitored with a signal analyzer having capability for real time power spectrum analysis. The accelerometers were located as shown on Figure 16. One vertically oriented accelerometer was placed in the aircraft model on the cavity forward bulkhead (the cavity was closed), and a laterally oriented accelerometer was also placed at this location. Additionally, two lateral accelerometers were placed on the sting; one at the tethered end and one near the sting mid-length.

1. Measurements from Manual Excitation of the Model

Measurements were initially taken with no air loading by manually shaking the model for both the no-tether and with-tether cases. Plots of the power spectrum measurements for the model cavity vertical and horizontal accelerometers are given in Figures 17 and 18, respectively, for the no-tethers case for a 0. to 10. Hz frequency range. All amplitudes in these plots and subsequent plots are shown in root-mean-square volts squared where one volt corresponds to a one G acceleration. Resonance peaks are labeled with the measured frequency and likely corresponding mode shape, i.e. the finite element model mode shape most likely to agree at that measured frequency. Plots 19 and 20 show the same measurements but with the tethers connected (here the frequency range was from 0.5 to 10.5 Hz so to eliminate any analyzer error in attempting to calculate a power spectrum level at zero Hz).

These measurements were taken to gain insight into the modal behavior of the system and the effect of the tethering system upon that behavior. The response peaks measured correlate well to the modes predicted by the finite element model with the main difference being that the lateral modes are lower in frequency than

that expected (e.g. 0.962 Hz for measured lateral bending vs. 1.26 Hz predicted lateral bending with no tethers). The shift of the no-tethers lateral bending mode from 0.962 Hz to a with-tethers combined lateral/torsion mode at 3.088 Hz was in stark agreement with the finite element model (FEM) predictions. The occurrence of both the lateral/torsion mode and vertical bending mode near the 3 Hz frequency point correlated well to the FEM prediction. (The vertical bending mode was measured at 3.413 Hz in the with-tethers case and at 2.987 Hz with the no-tethers case. This shift is believed due to having the vertical load compensation system active in the with-tethers case and not active in the no-tethers case. This frequency shift was seen later during air loading runs, and the load compensation system effects were not included in any of the FEM analysis.)

Structural damping estimates were desired for the various resonance modes so that changes in damping could be monitored during the tunnel envelope check run. An effective structural damping estimate of 4.0% was made on the lateral/torsion mode peak in the with-tethers case (see Figure 20) using the peak-picking method. This method approximates the structural damping at a resonance by dividing the peak's half-power point bandwidth by that peak's resonance frequency. The method assumes a uniform random noise input over the frequency range of the normal mode, a structural damping level less than 10%, an analysis resolution bandwidth much smaller than the half-power point bandwidth (a ratio on the order of 0.2 or less), and that the resonance mode does not overlap heavily with neighboring modes. (See Engineering Applications of Correlation and Spectral Analysis, by Bendat and Piersol). The 4.0 % estimate made in this no-air loading, manual excitation case is crude because the input was intended to excite this particular mode and to maintain its amplitude, which is far different than inputting uniform random noise. Otherwise the estimate would have been reasonable since the analysis resolution bandwidth to half-power point bandwidth ratio was 0.0125 Hz/0.125 Hz or 0.1, no neighboring modes heavily overlapped this mode (the vertical bending mode, though neighboring closely in frequency, does not have any significant lateral acceleration component that would be seen in this particular measurement), and the resulting 4% damping estimate is below the 10% limit for method accuracy. Though crude, the 4% estimate did give a preliminary ballpark figure for the damping levels present in the system.

Measurements taken on the two sting mounted accelerometers (#3 and #4 of Figure 16) showed no new information regarding the low frequency modes and insufficient input was applied with the manual excitation to obtain clean measurements of higher frequency modes.

2. Measurements During the Check-Out Run

The model/sting response was monitored in a check-out run covering the range of airspeed and model angle of attack intended for the subsequent model testing.

a. Low-End Mach Number Sweep

The model/sting system was first checked out for zero angle of attack at Mach numbers progressing through 0.3, 0.4, 0.5, 0.6, and 0.75 settings. The model/sting response was monitored between frequencies of 0.5 and 32.5 Hz so higher frequency modes could be tracked for any indications of flutter behavior. Accelerometers #1 and #2 were tracked primarily and power spectrum plots were made for these at all test points. Accelerometers #3 and #4 were monitored secondarily, and the output from these accelerometers was recorded only at the Nm = 0.5 point. Figures 21 through 29 show the recorded output from this portion of the test envelope check-out.

A plot of peak response, damping estimate, and frequency versus Mach number was made for the two low frequency modes. These are shown in Figures 30 and 31. Response amplitude growth with Mach number for these two modes was very stable and damping appeared to increase. Frequencies shifted downward for both modes with the vertical bending mode frequency going below that of the lateral/torsion mode.

A plot of amplitude and frequency of one of several modes around the 20 Hz range did show amplitude growth greater than linear growth and an apparent increase in frequency. See Figure 32 for this plot. Some coalescing of modes in this frequency range was thought possible from the data plots (compare Figure 28 to Figure 21). System response in this frequency range was subsequently monitored with equal attention as the lower frequency modes.

b. Angle of Attack Sweep for Low-End Mach

Angle of attack variations were run in the 0.5 to 0.75 Mach number regime. The angle was swept was between 0 and 5 degrees at Nm = 0.5 and no significant change in system modal response was observed. A constant angle of attack of 2.5 degrees was set and the Mach number was run back up to 0.75 with no significant changes. Power spectrum plots were made for these runs but are not included in this report.

c. High-End Mach Number Sweep

Having seen no divergent growth in resonance amplitudes nor significant loss in modal damping, the model/sting system was then monitored for the remainder of the test envelope Mach range. The angle of attack was set to zero and the Mach number increased from 0.75 through settings of 0.79, 0.82, 0.85, and 0.88. See Figures 33 through 37 for power spectrum plots of accelerometers #1 and #2 for these test points. No divergent growth of resonance peak amplitudes was observed, and the modes in the 20 Hz range appeared to diminish and wash out rather than grow further. The response peak of the system for the lateral/torsion rocking (the first large peak for accelerometer #2 on Figure 37) did appear somewhat sharpened and higher in amplitude at the 0.88 Mach point setting. The damping level of this peak was judged still well within reasonable bounds and no higher Mach number is intended for the test envelope. The behavior of this peak and the peak for the vertical bending mode were monitored closely in subsequent angle of attack sweeps at high Mach numbers.

Additionally, a power spectrum in rms volts for the 30 through 230 Hz frequency range was made for the #1 and #2 accelerometers for an angle of attack equal to zero and at Mach 0.88. This plot, seen in Figure 38, provides indication of power spectrum levels at higher frequencies where test measurements upon the telescope model are planned.

d. Angle of Attack Sweep for High-End Mach

Angle of attack sweeps were then run from 0 to 5 degrees at Mach points 0.79 and 0.82. Angle of attack sweeps from 0 to 4 degrees were run for points 0.85 and 0.88 (the 5 degree point was not run for the last two Mach points because of lift loads being higher than expected and near the design limit at 4 degrees). Figures

39 through 43 show the power spectrum plots for accelerometers #1 and #2 for these test points. Amplitudes, frequencies and damping were monitored throughout these sweeps. No unusual amplitude growth or frequency shifts were observed.

Damping was monitored closely through the alpha sweeps for the high-end Mach numbers, and estimates ran between 3.1 and 8.1 %. The higher damping estimates were usually for the first peak of the #1 accelerometer, which measured vertical accelerations in the cavity area of the aircraft model. This accelerometer was subject to accelerations from both the vertical bending and lateral/torsion modes. Because these two modes were consistently closely spaced in frequency, the damping estimate is subject to significant error (in effect the single peak used for damping estimation is actually a double peak spanning two modes).

For all the measurements taken over the 0.5 to 32.5 Hz frequency range, the frequency resolution to half-power point bandwidth ratio was on the order of 0.32 to 0.36, which is greater than the recommended 0.2 or less. The result is that the damping estimates are somewhat imprecise and useful in more of a qualitative sense for monitoring relative change.

e. Damping Estimate for Worst Case Conditions

The final measurement at 4 degrees angle of attack and Mach 0.88 was repeated for a 0.5 to 10.5 Hz frequency range and for 8 time averages so to increase the frequency resolution and attempt to get an accurate damping estimate at worst case tunnel/model conditions. The results of this data run are shown in Figure 44 and shown again in Figure 45 on a magnified amplitude scale.

These plots show many closely spaced slender peaks, which if taken individually as separate modal peaks, show modes with damping around 1.5%. The reason for the spikiness of the power spectrum curve is unclear. A greater number of time averages would help to reduce the noise effects remaining after 8 averages, but these effects may not be the cause of the spikiness. Nonlinearities in the structure, primarily from the vertical support strut drive and hysteresis in the joints, may cause the resonance frequency to incrementally shift so that no clear single peak emerges. The effective damping of a mode assumed to have no nonlinearities is difficult to estimate from such plots and may be best

estimated by observing the nonlinear peaks with a reduced frequency resolution (as was done for most of the check run with the 0.5 to 32.5 Hz power spectrum plots).

IV. Conclusions

The model/sting system did not diverge nor flutter in the test envelope check-out run, which other than for yaw angle changes, covers the test envelope range intended for the SOFIA model test. This was obvious to all whom observed the model during the run, irrespective of these measurements. No strong indications of the onset of flutter occurred during the power spectrum measurements, though the conditions for heightened concern did occur and were monitored for their development.

STING / MODEL SYSTEM
FINITE ELEMENT MODEL

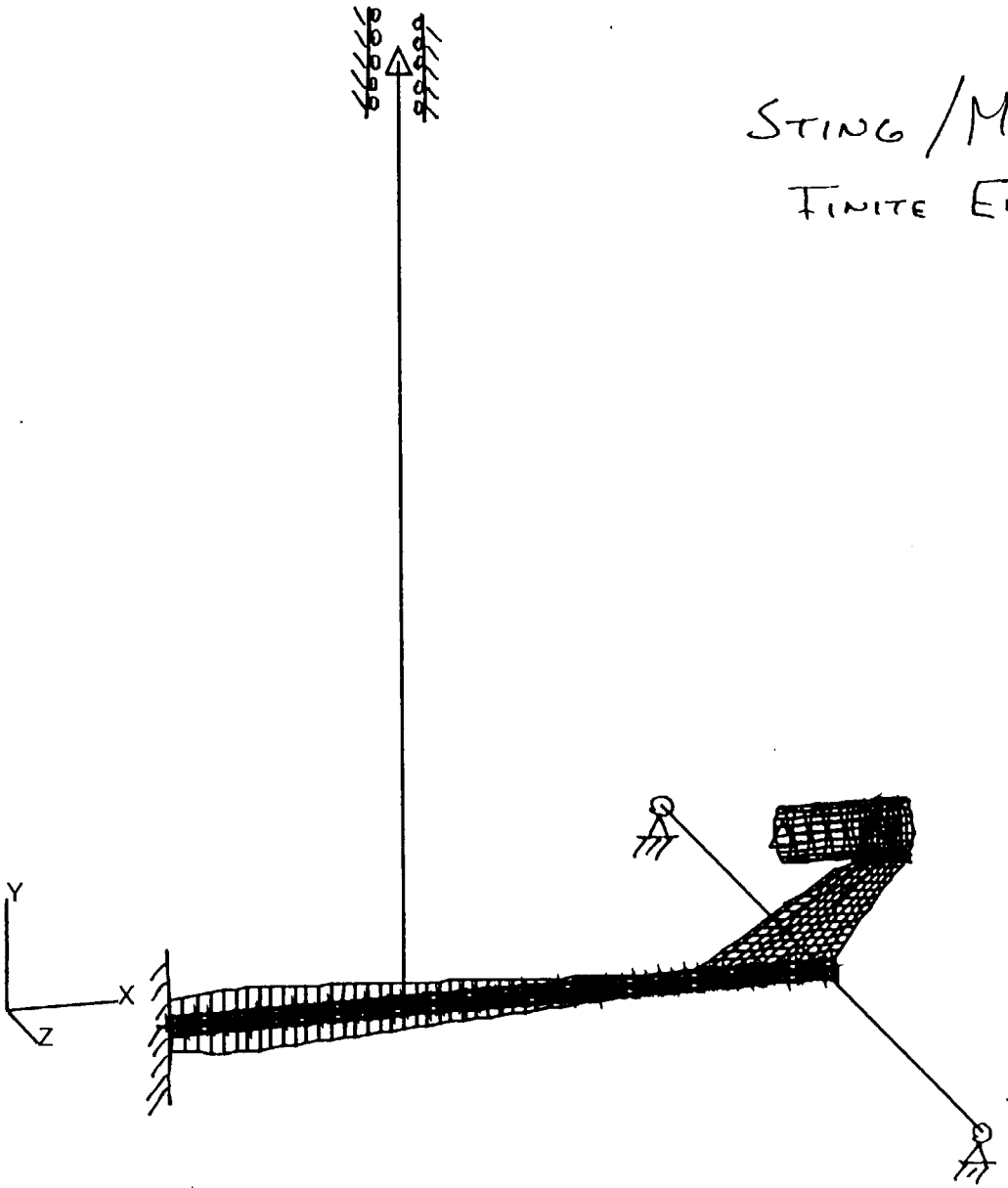

FIGURE 1

STING, BLADE, AIRCRAFT MODEL REPRESENTATION

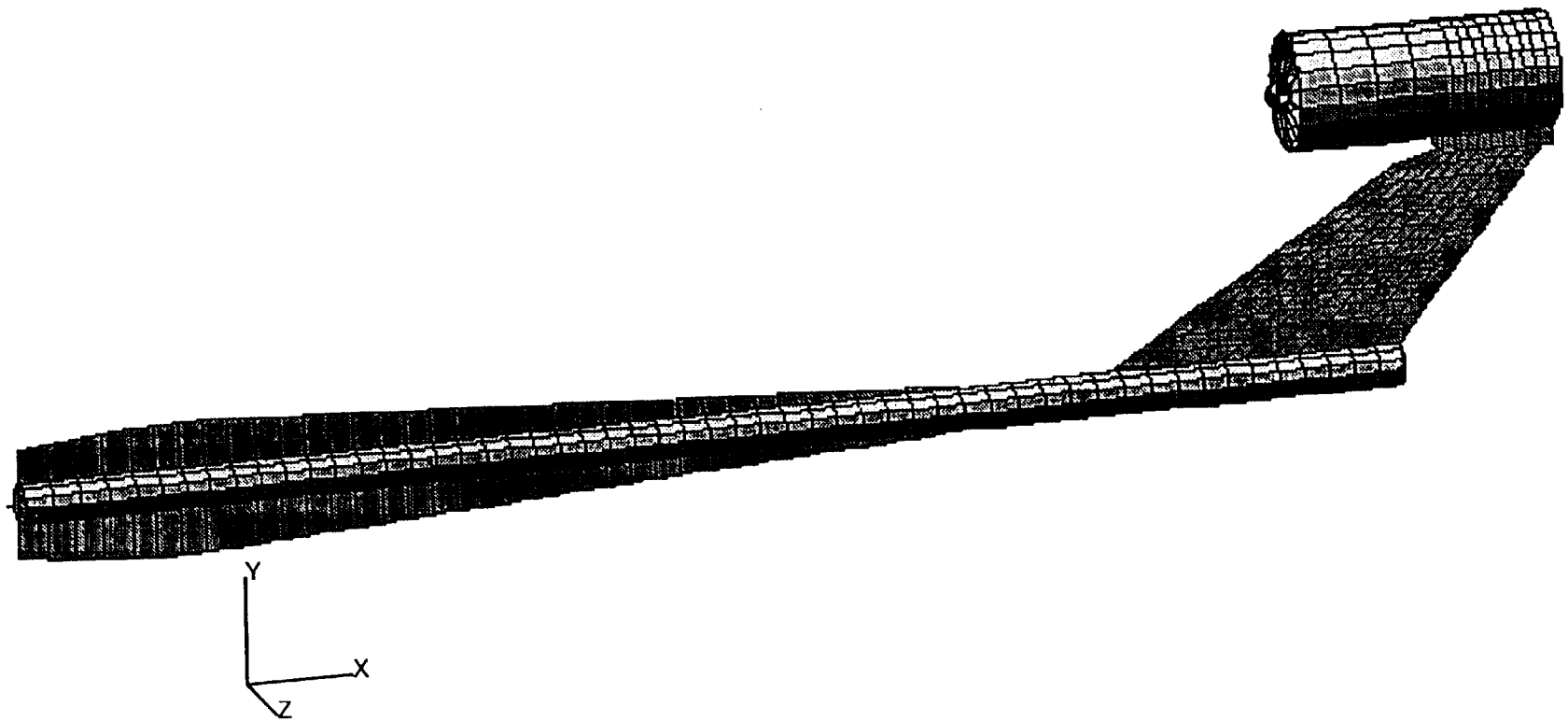

FIGURE 2

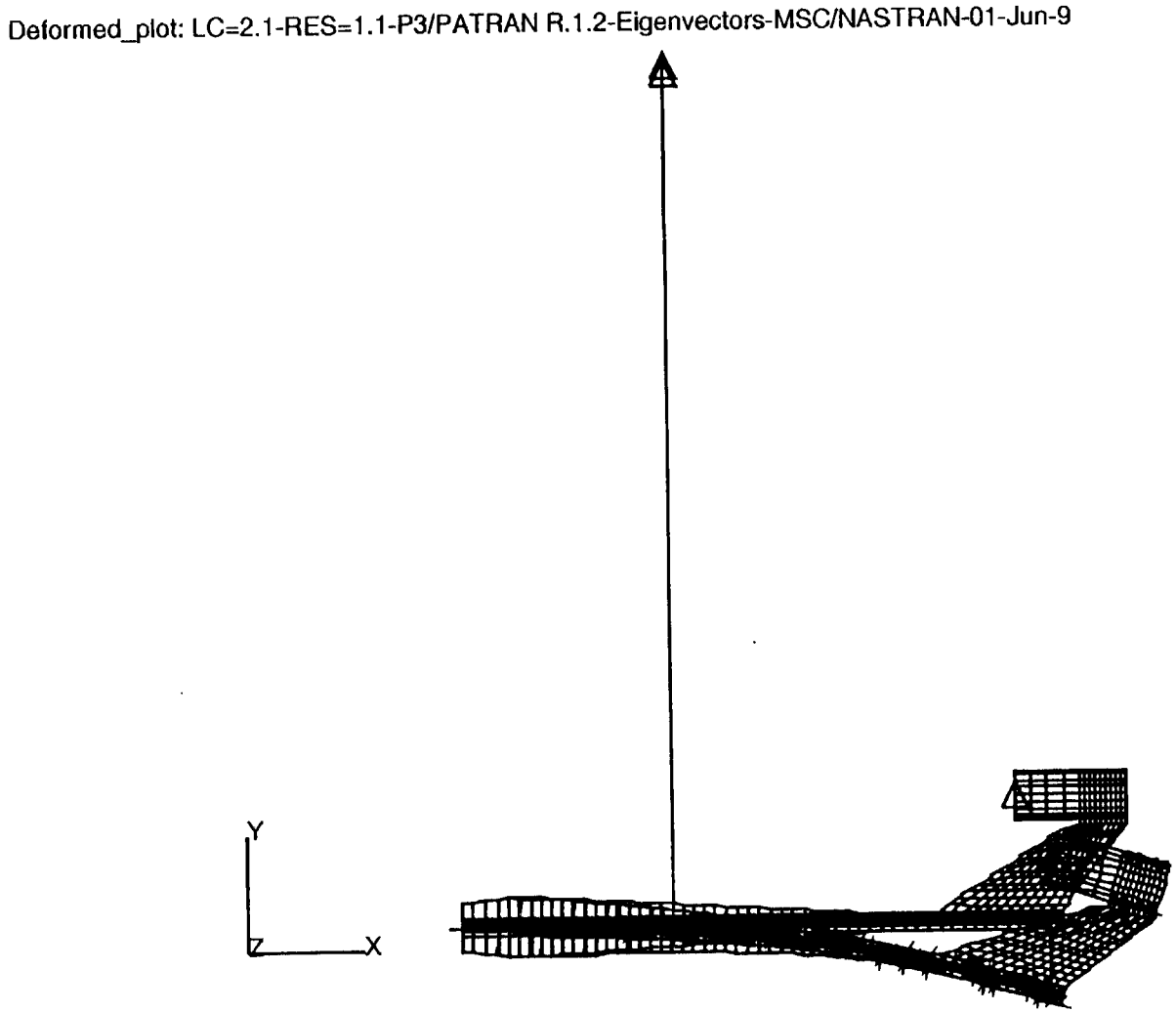

FIGURE 3, MODE 1, $f_1 = 3.000$ Hz

Deformed_plot: LC=2.2-RES=1.1-P3/PATRAN R.1.2-Eigenvectors-MSC/NASTRAN-01-Jun-9

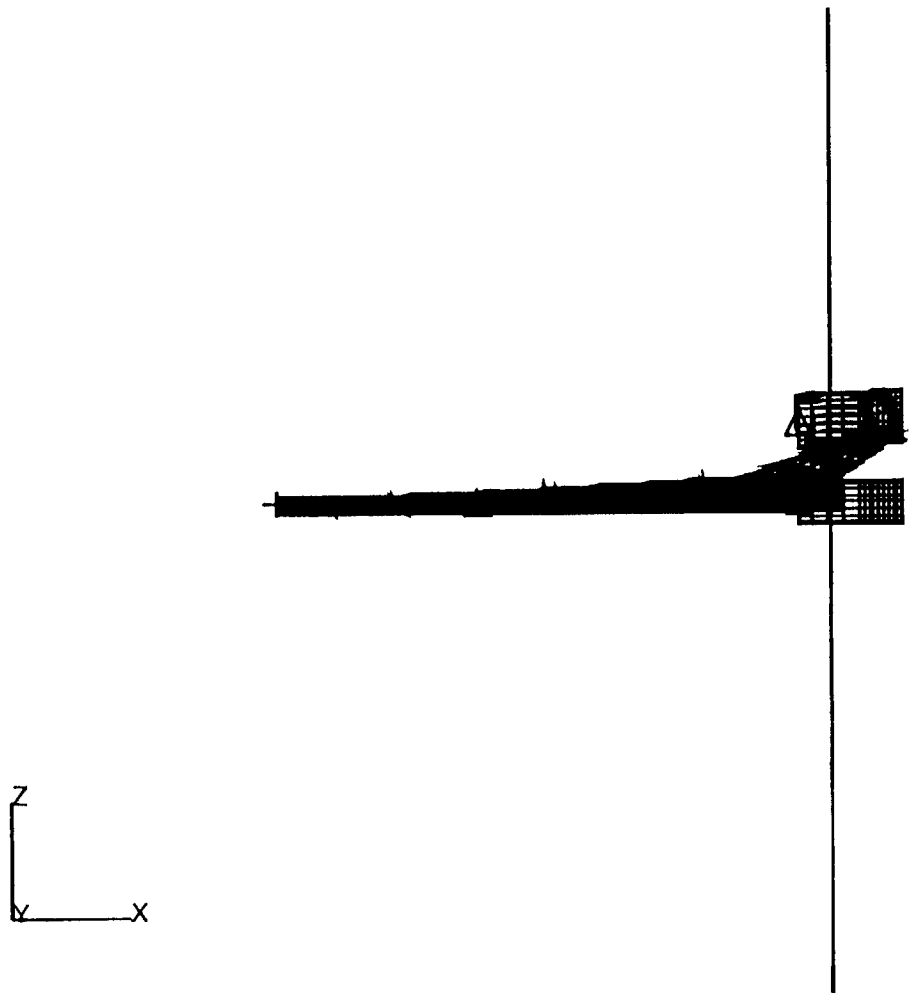

FIGURE 4, MODE 2, $f_2 = 3.033$ Hz

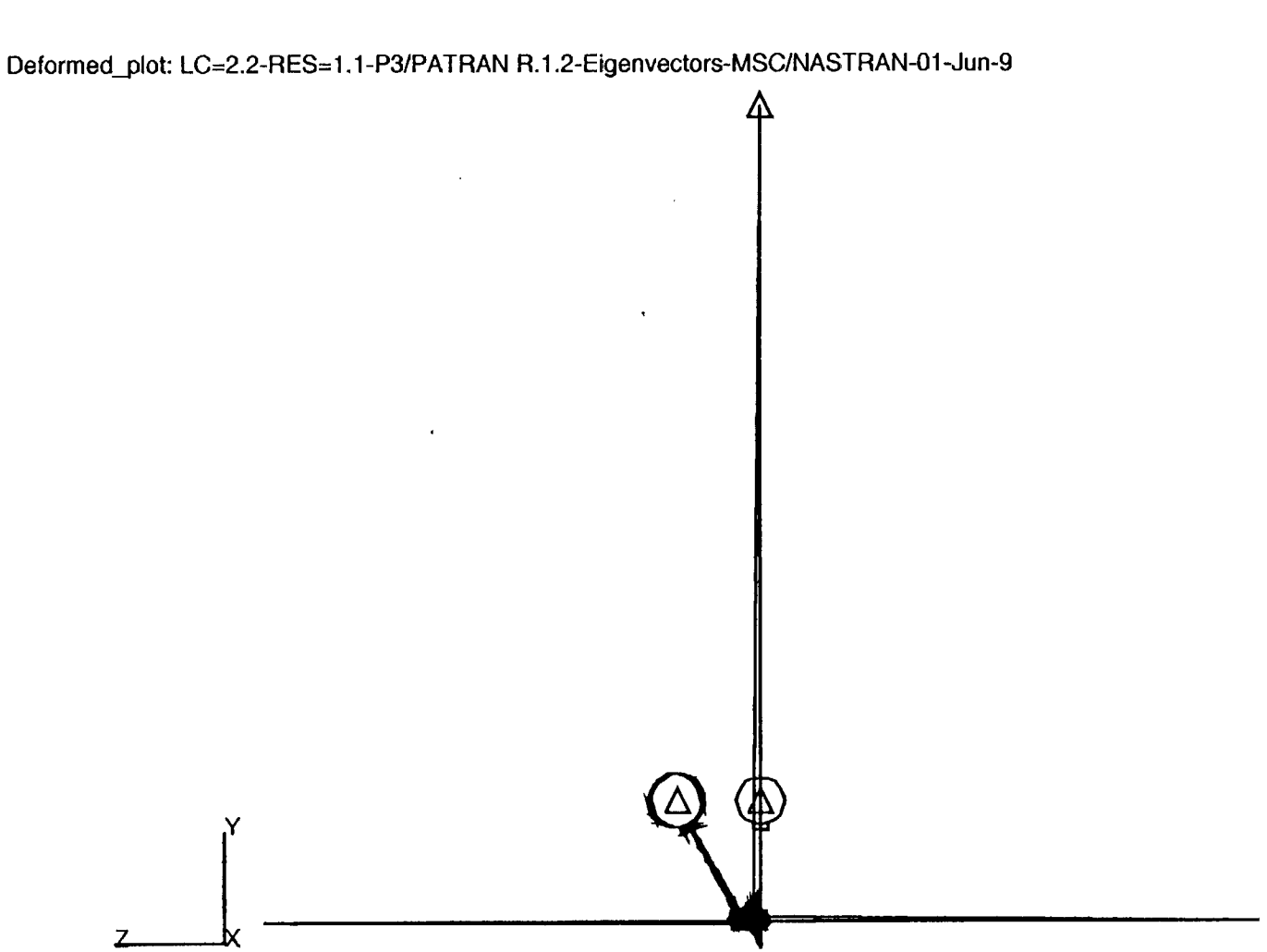

FIGURE 5, MODE 2, $f_2 = 3.033$ Hz

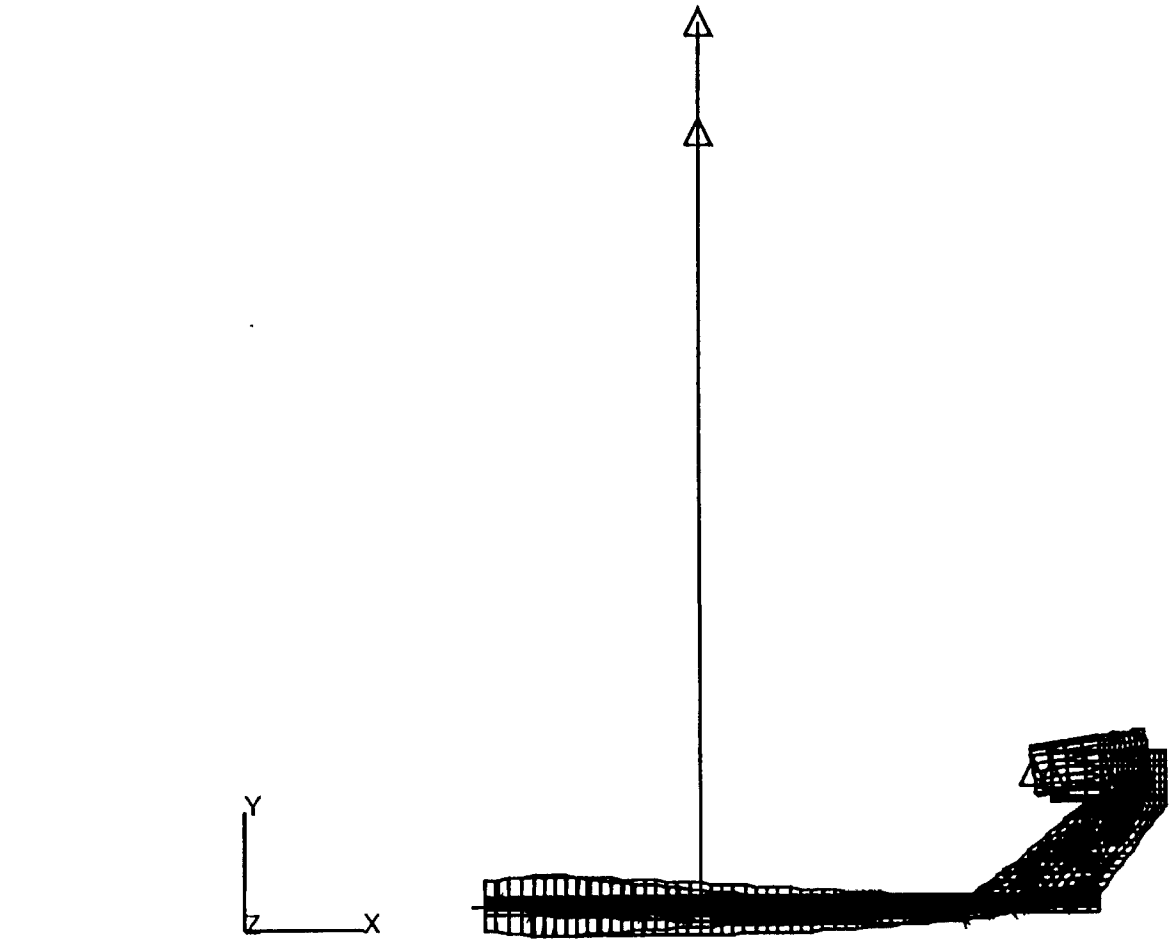

FIGURE 6, MODE 3, $f_3 = 5.561$ Hz

Deformed_plot: LC=2.4-RES=1.1-P3/PATRAN R.1.2-Eigenvectors-MSC/NASTRAN-01-Jun-9

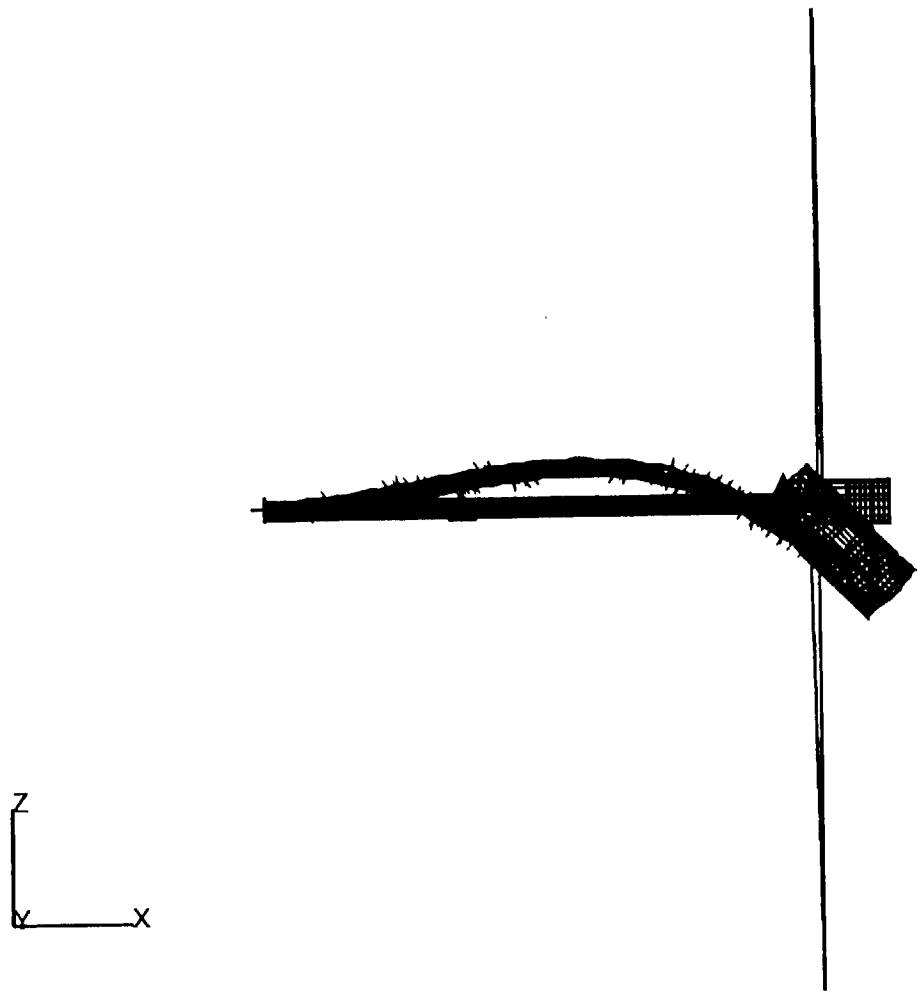

FIGURE 7, MODE 4, $f_4 = 6.447$ Hz

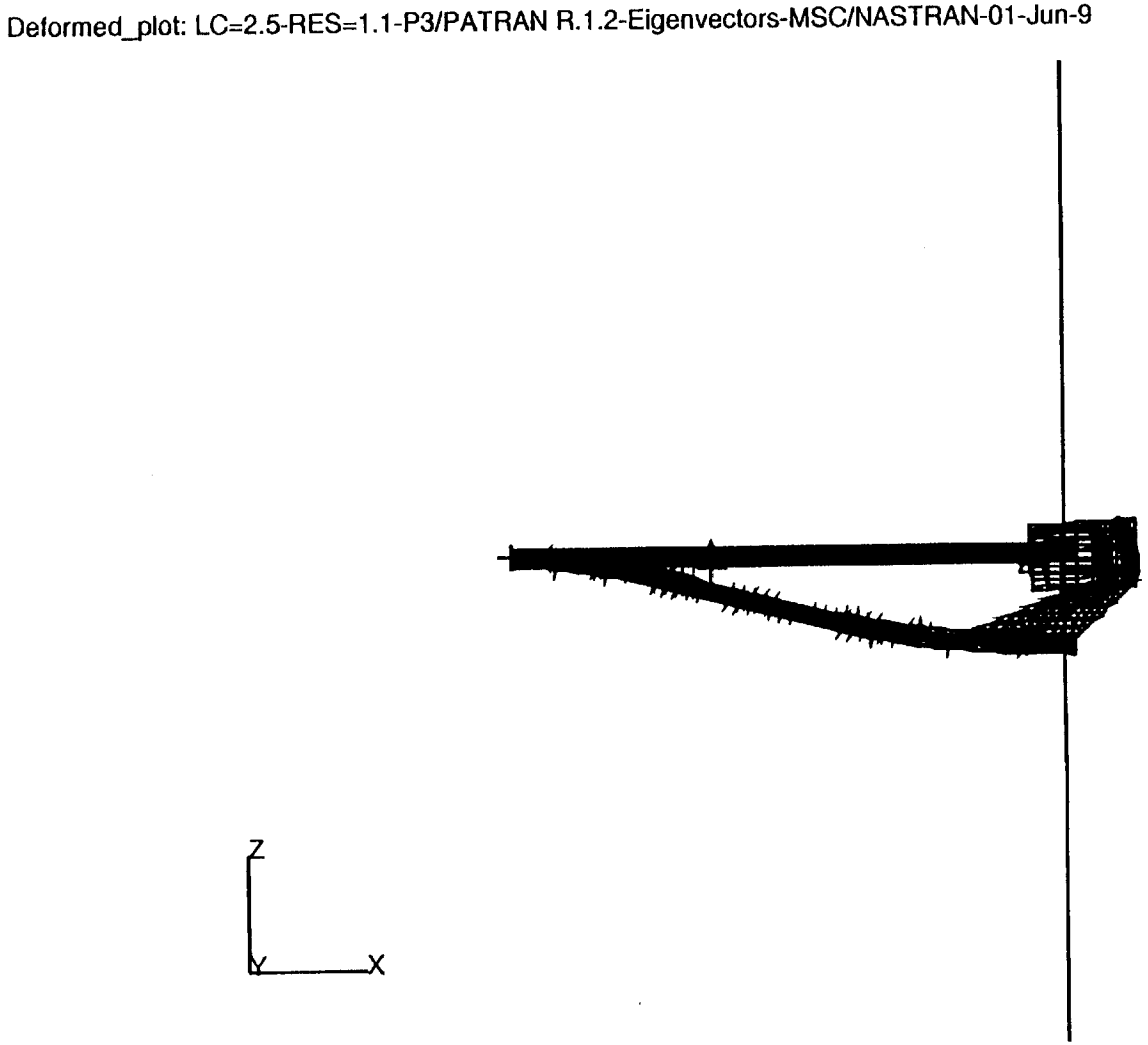

FIGURE 8, MODE 5, $f_5 = 9.152$ Hz

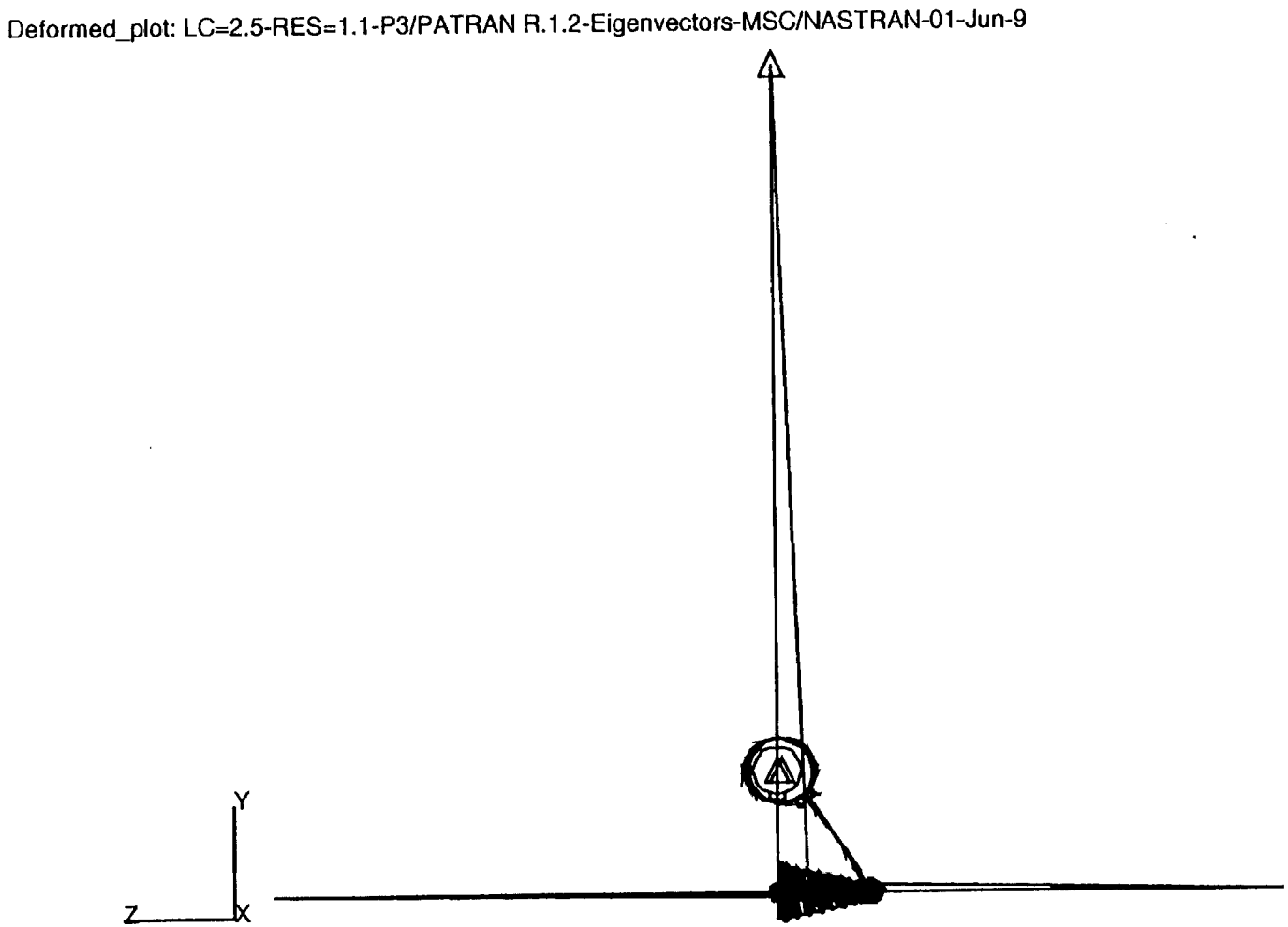

FIGURE 9, MODE 5, $f_5 = 9.152$ Hz

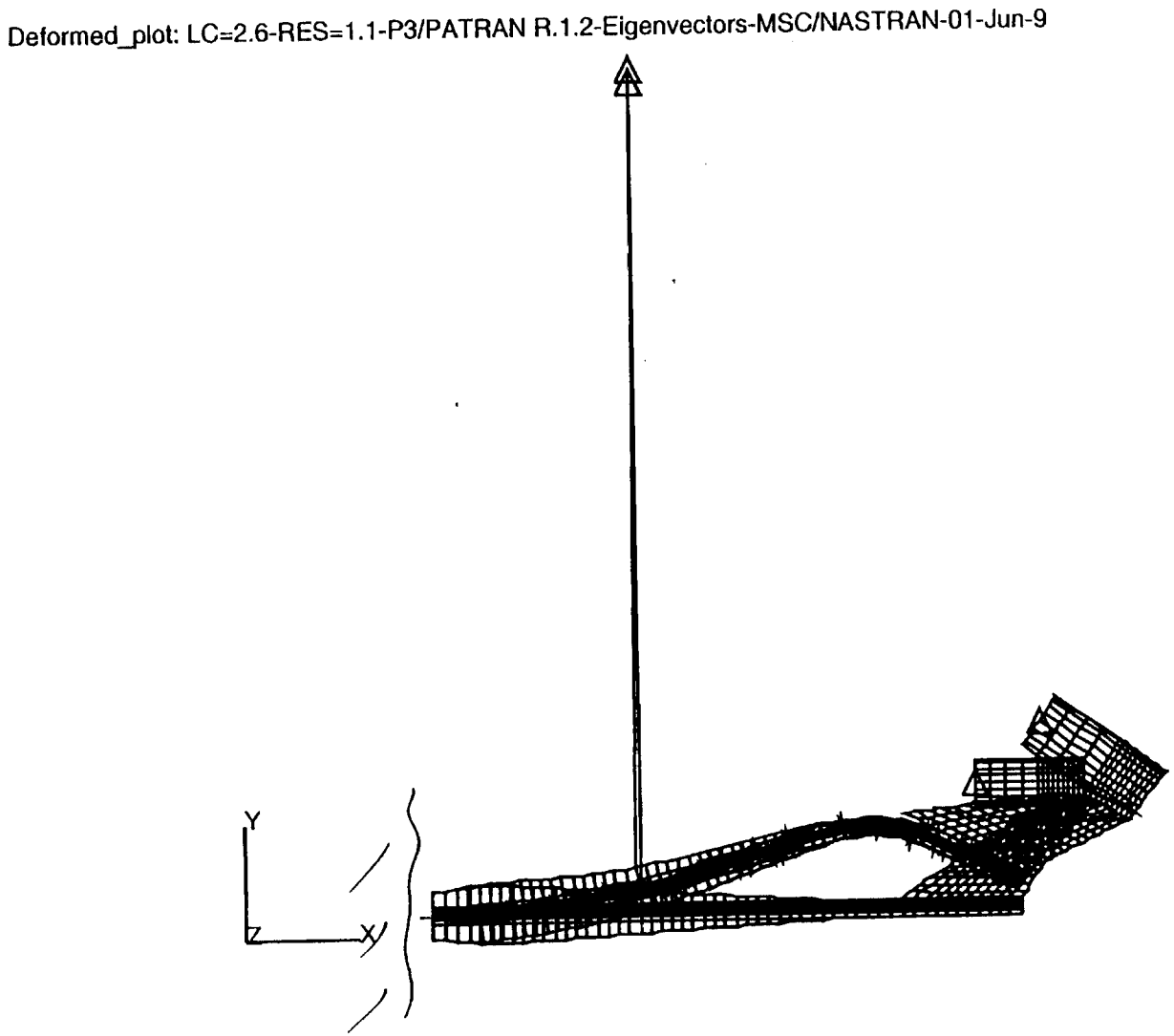

FIGURE 10, MODE 6, $f_6 = 9.980$ Hz

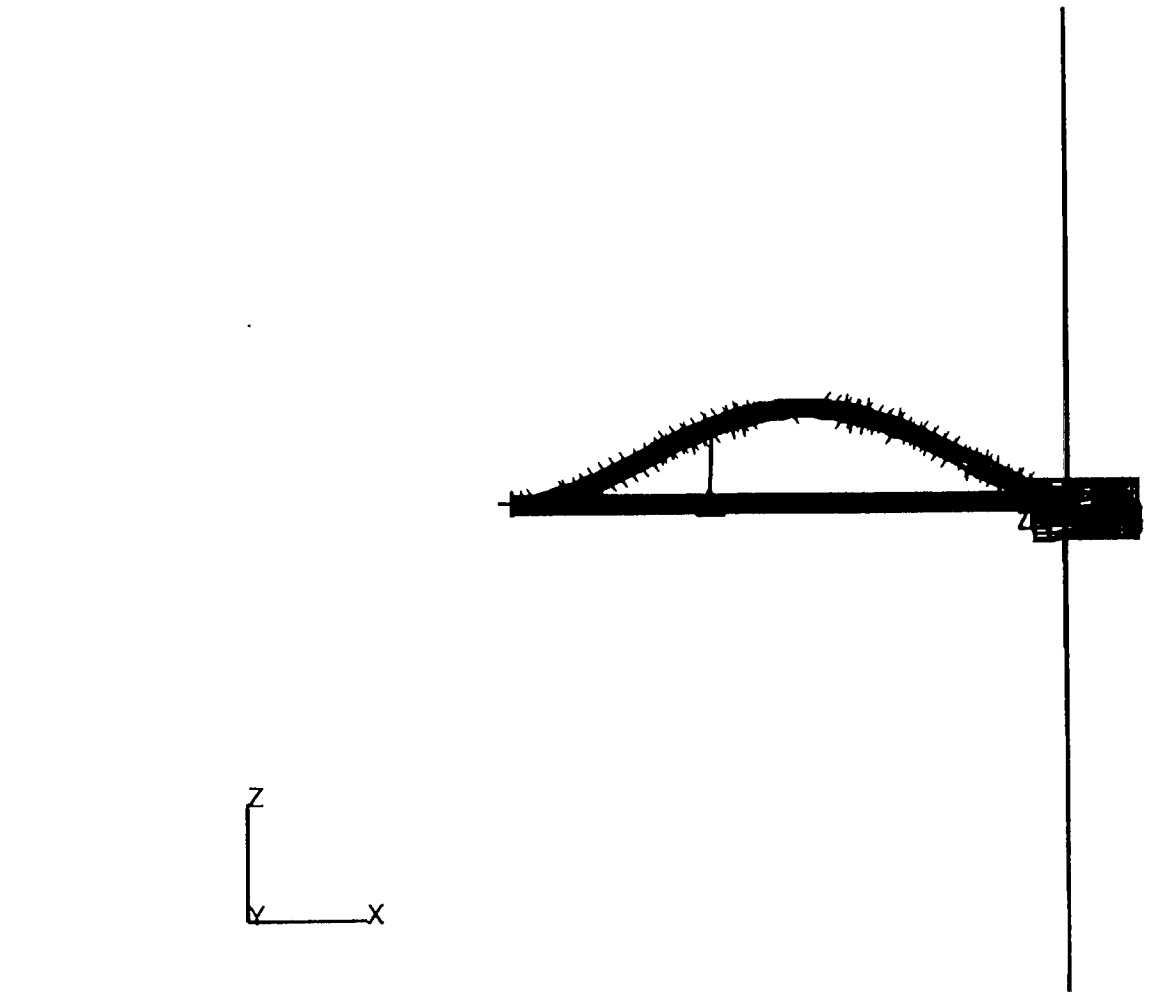

FIGURE 11, MODE 7, $f_7 = 20.96$ Hz

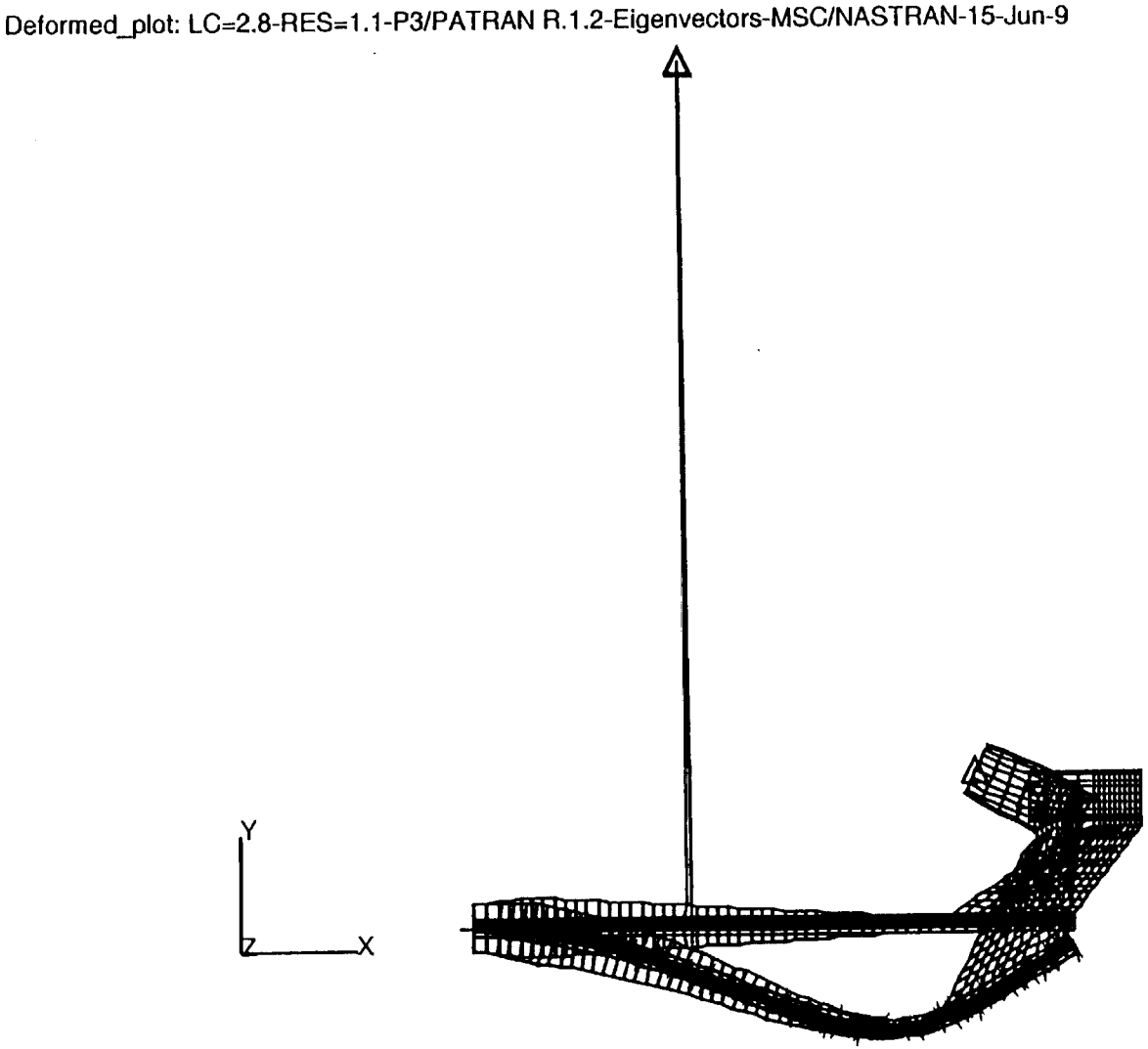

FIGURE 12, MODE 8, $f_8 = 32.38$ Hz

Deformed_plot: LC=2.1-RES=1.1-P3/PATRAN R.1.2-Eigenvectors-MSC/NASTRAN-01-Jun-9

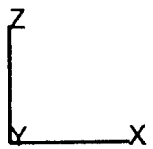

FIGURE 13, MODE 1 WITH NO TETHERS, $f_{1_{NT}} = 1.26$ Hz

Deformed_plot: LC=2.3-RES=1.1-P3/PATRAN R.1.2-Eigenvectors-MSC/NASTRAN-01-Jun-9

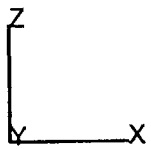

FIGURE 14, MODE 3 WITH NO TETHERS, $f_{3_{NT}} = 5.06$ Hz

Deformed_plot: LC=2.5-RES=1.1-P3/PATRAN R.1.2-Eigenvectors-MSC/NASTRAN-01-Jun-9

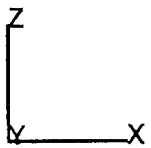

FIGURE 15, MODE 5 WITH NO TETHERS, $f_{S_{NT}} = 7.22$ Hz

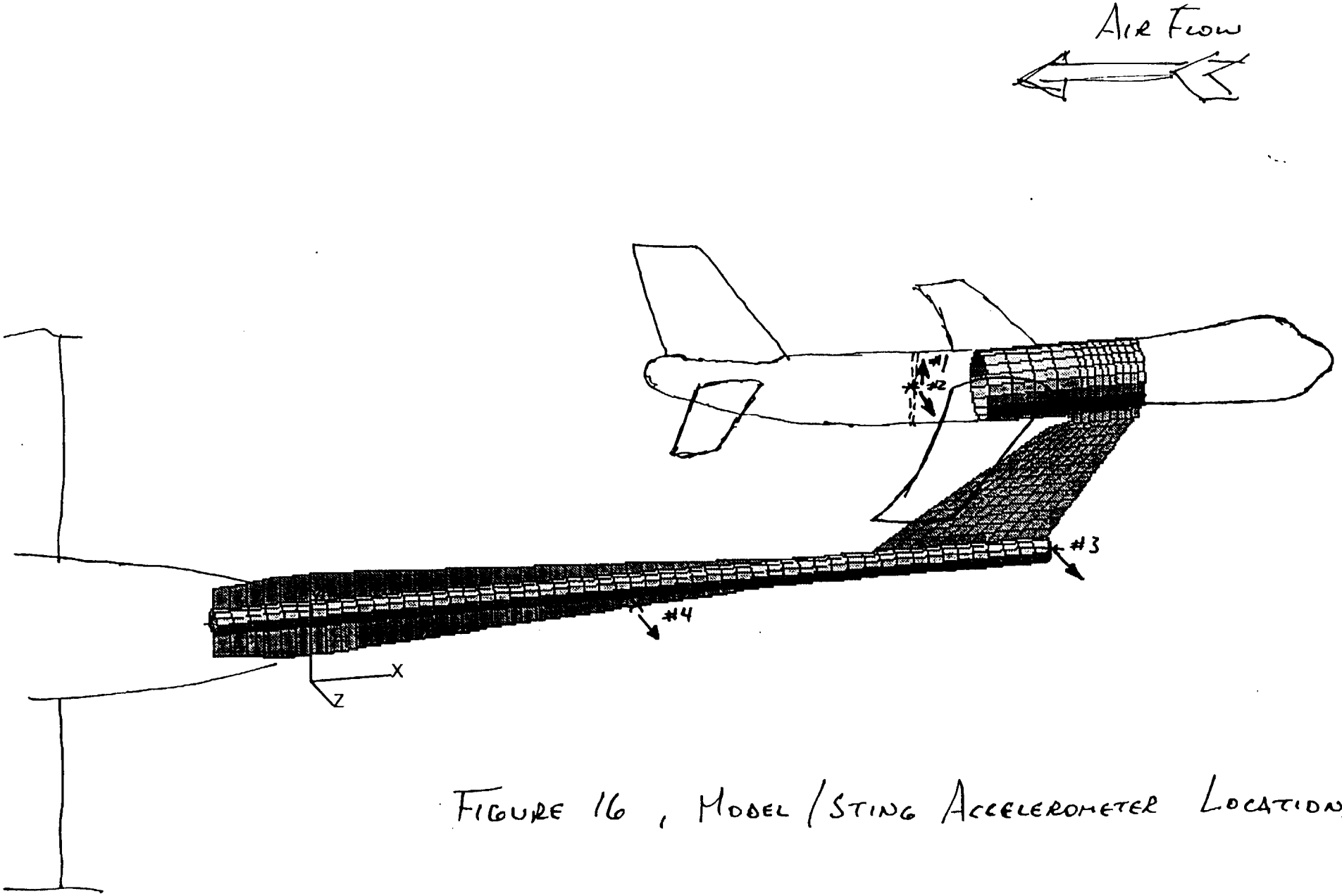

FIGURE 16, MODEL/STING ACCELEROMETER LOCATIONS

6-3-94 RGB

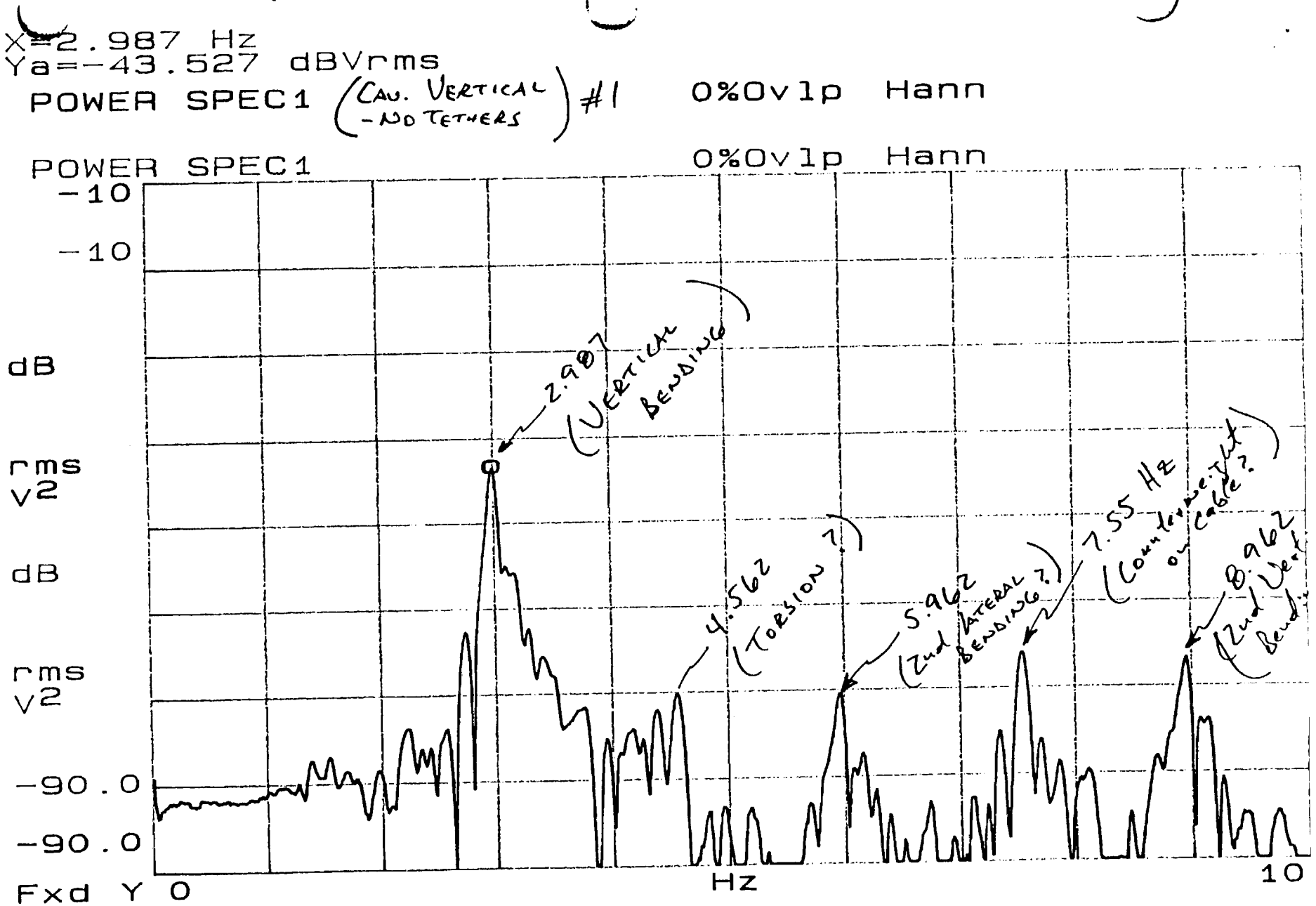

FIGURE 17, NO AIR LOADING, NO TETHERS, HAND SHAKEN

6-3-94 RGB

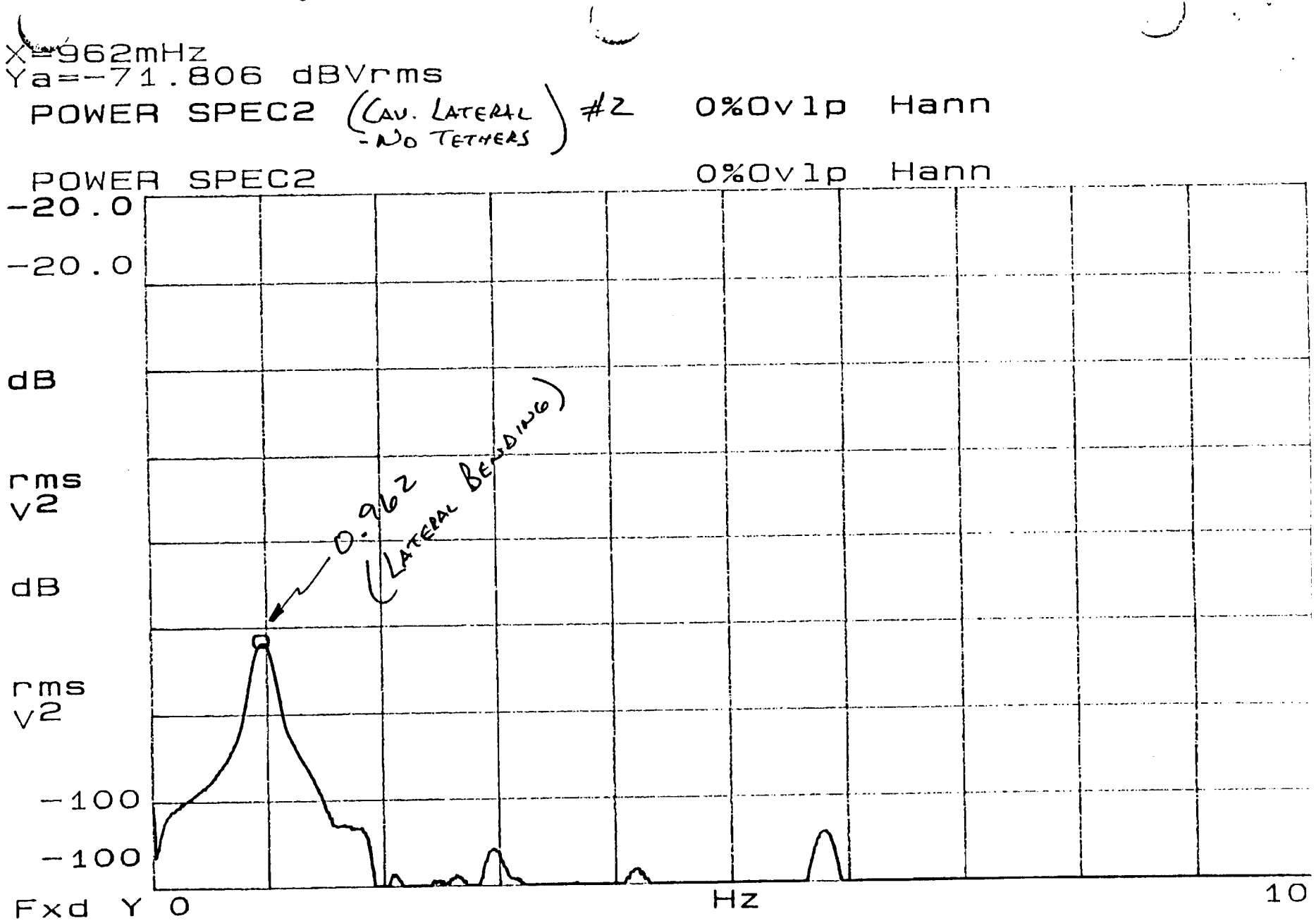

FIGURE 18, NO AIR LOADING, NO TETHERS, HAND SHAKEN

W/ TETHERS, NO AIR, HAND ROCKED AT WING.

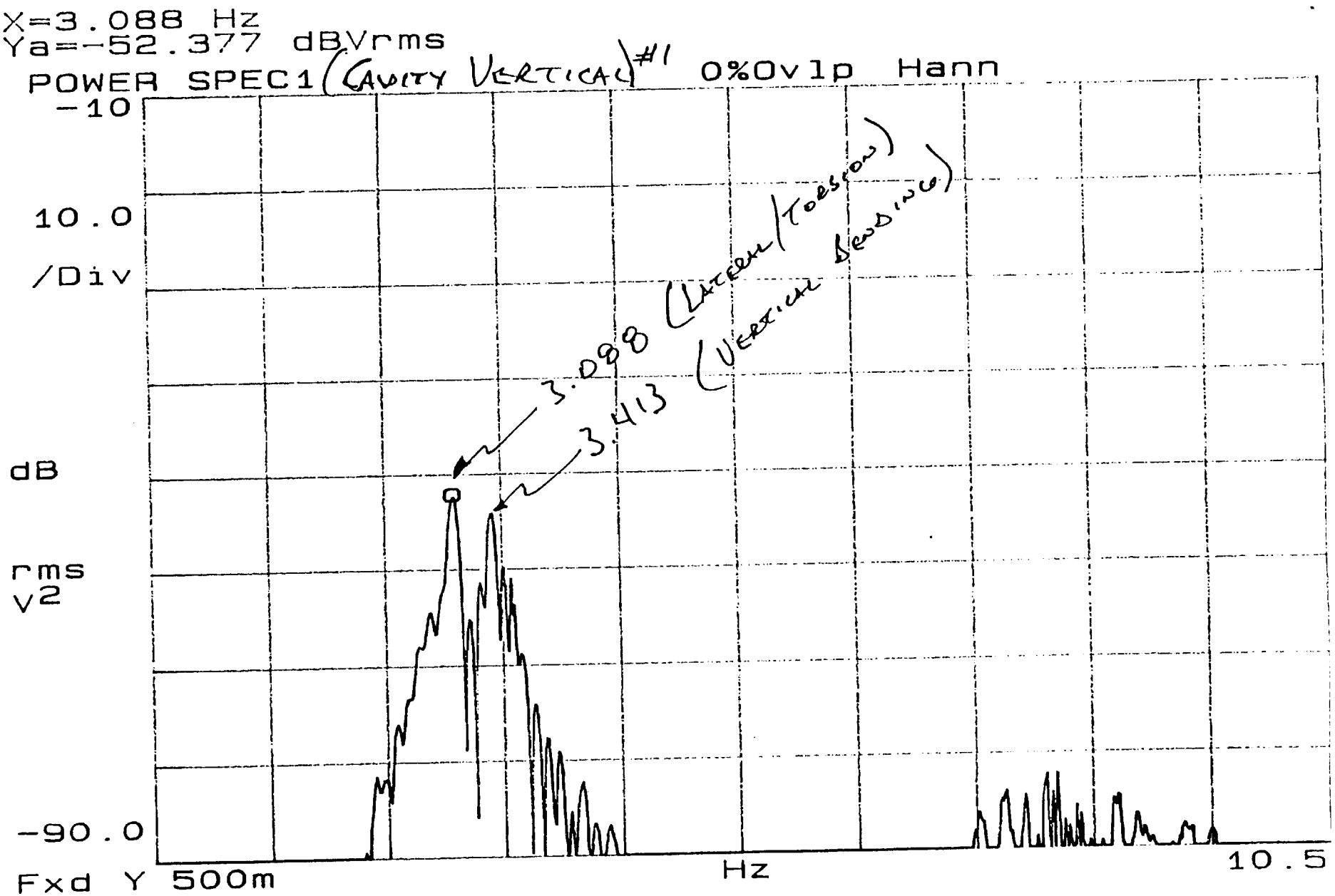

FIGURE 19, NO AIR LOADING, WITH TETHERS, HAND SHAKEN

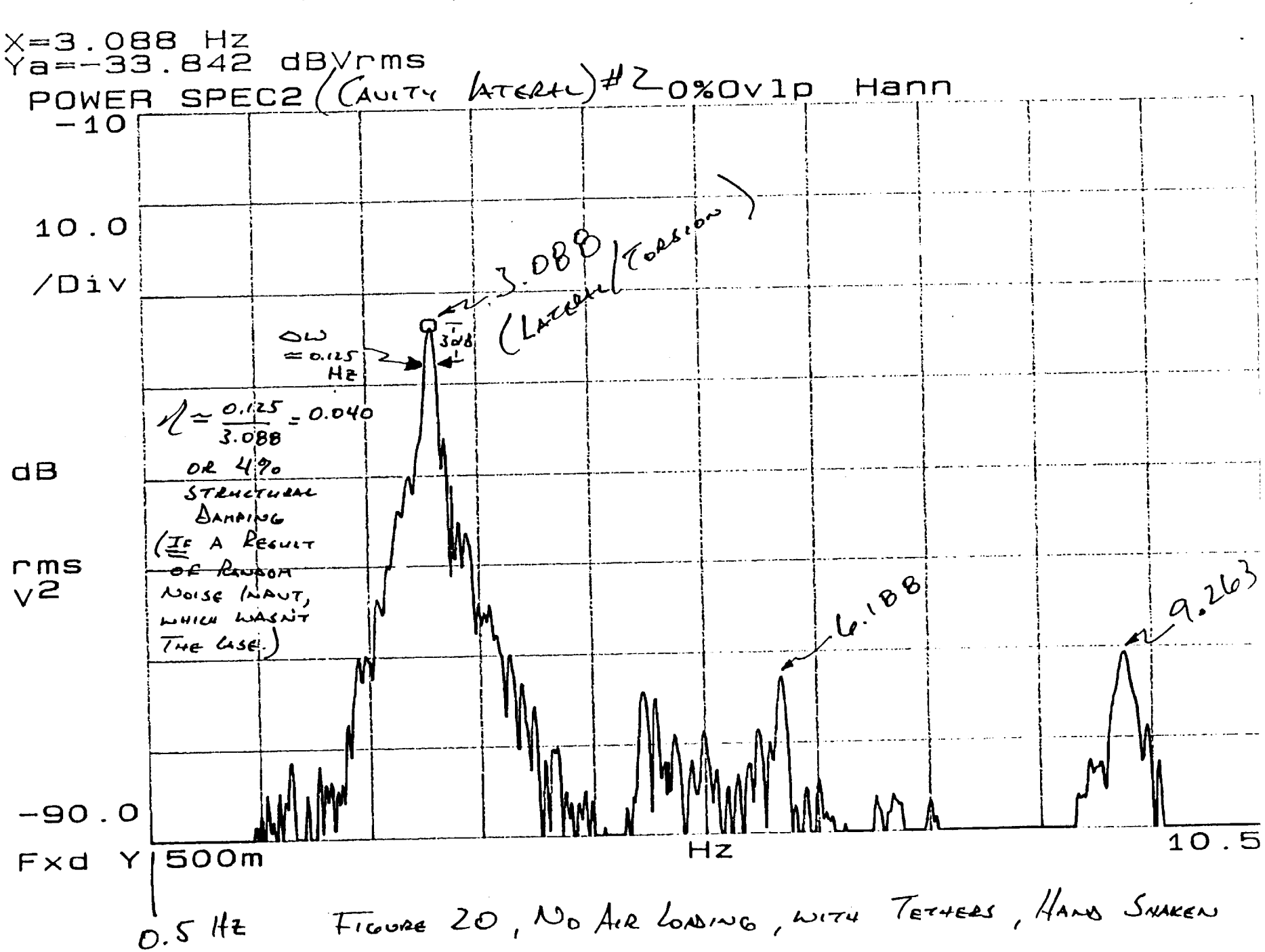

FIGURE 20, NO AIR LOADING, WITH TETHERS, HAND SHAKEN

6/7/94

$N_M = 0.4$

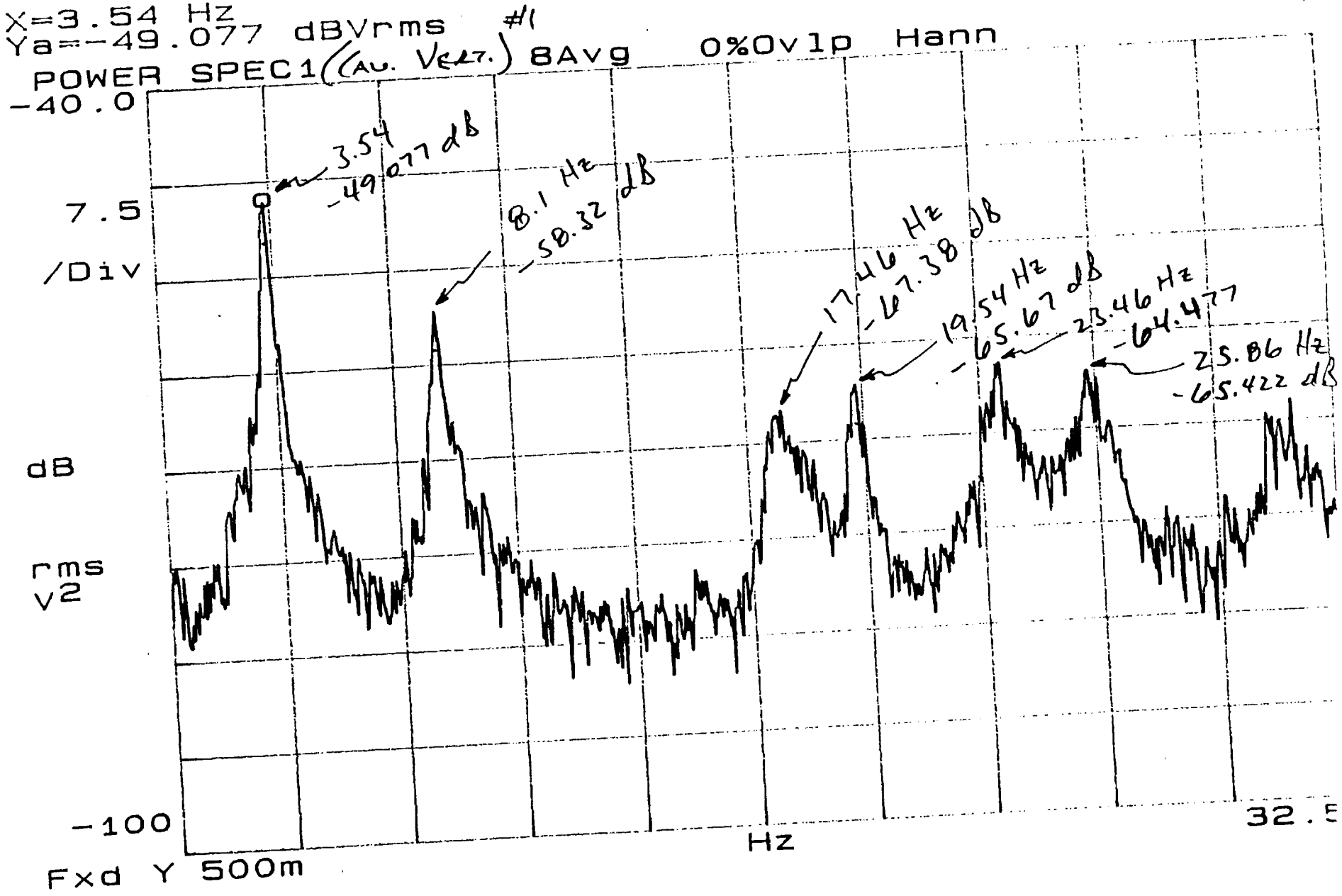

Figure 21

6/7/94

$N_M = 0.4$

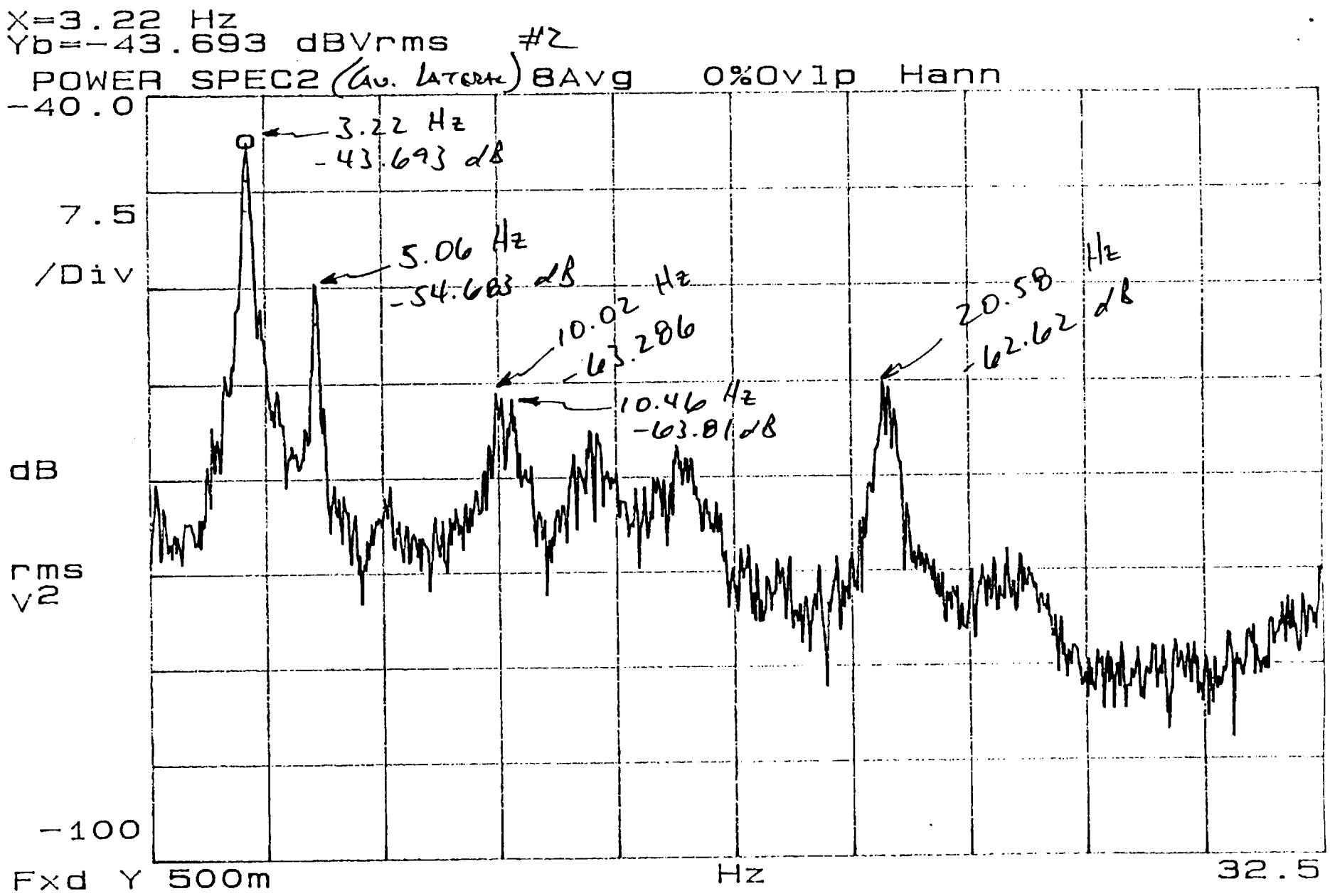

FIGURE 22

6/8/94 $N_m = 0.5$ $\alpha = 0^\circ$

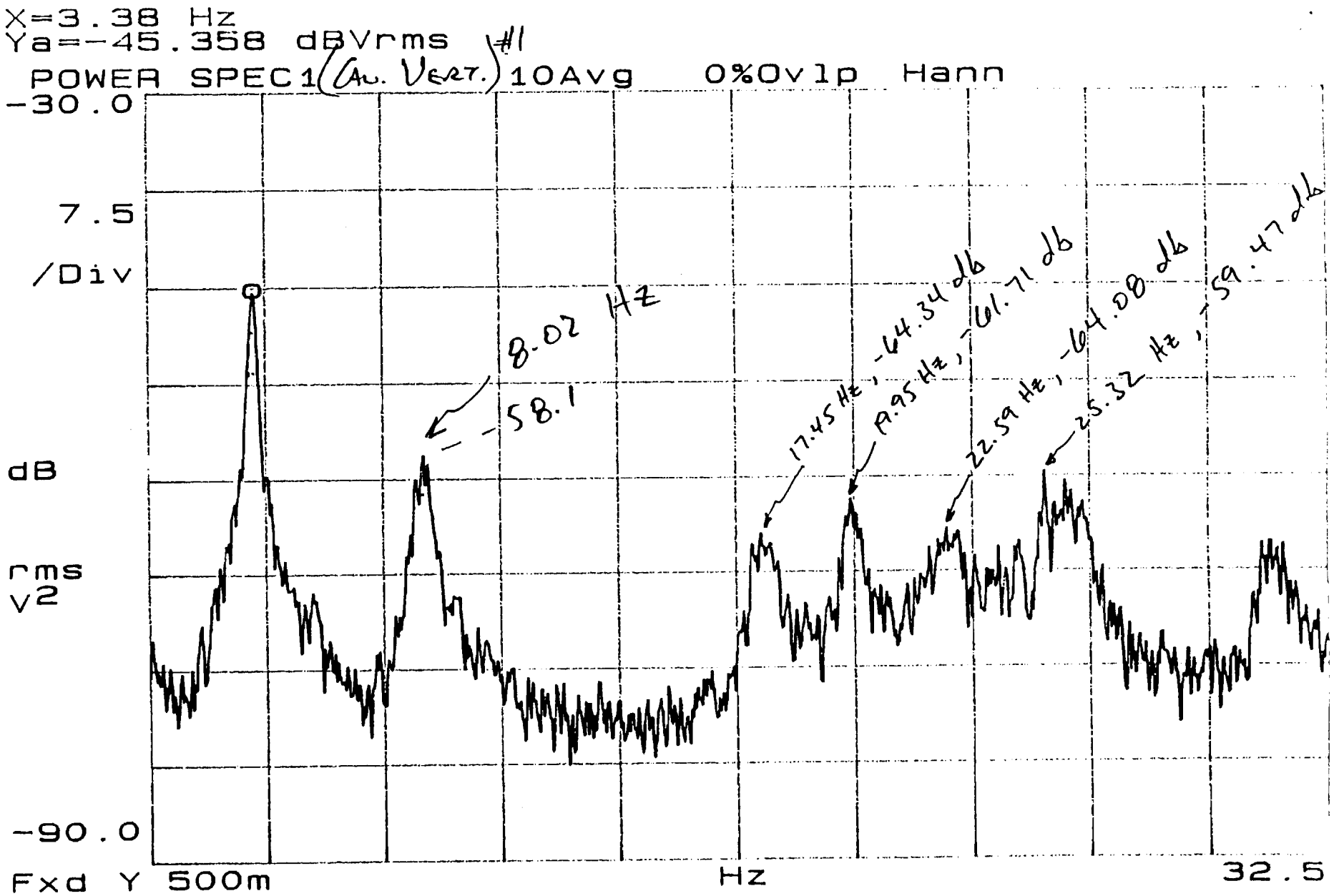

FIGURE 23

6/8/94 $\nu_n = 0.5$ $\alpha = 0$

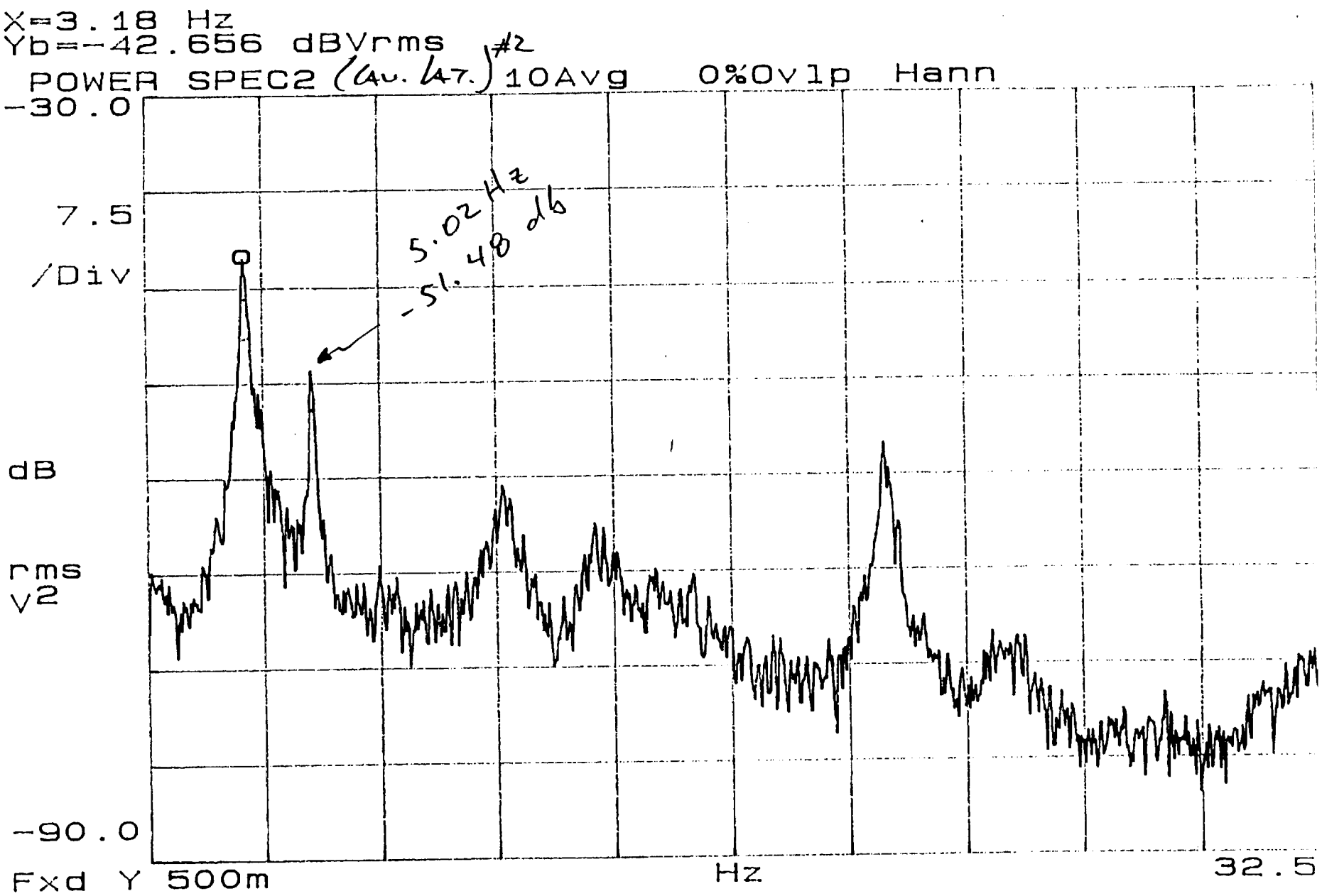

FIGURE 24

$\nu_n = 0.5 \quad \alpha = 0$

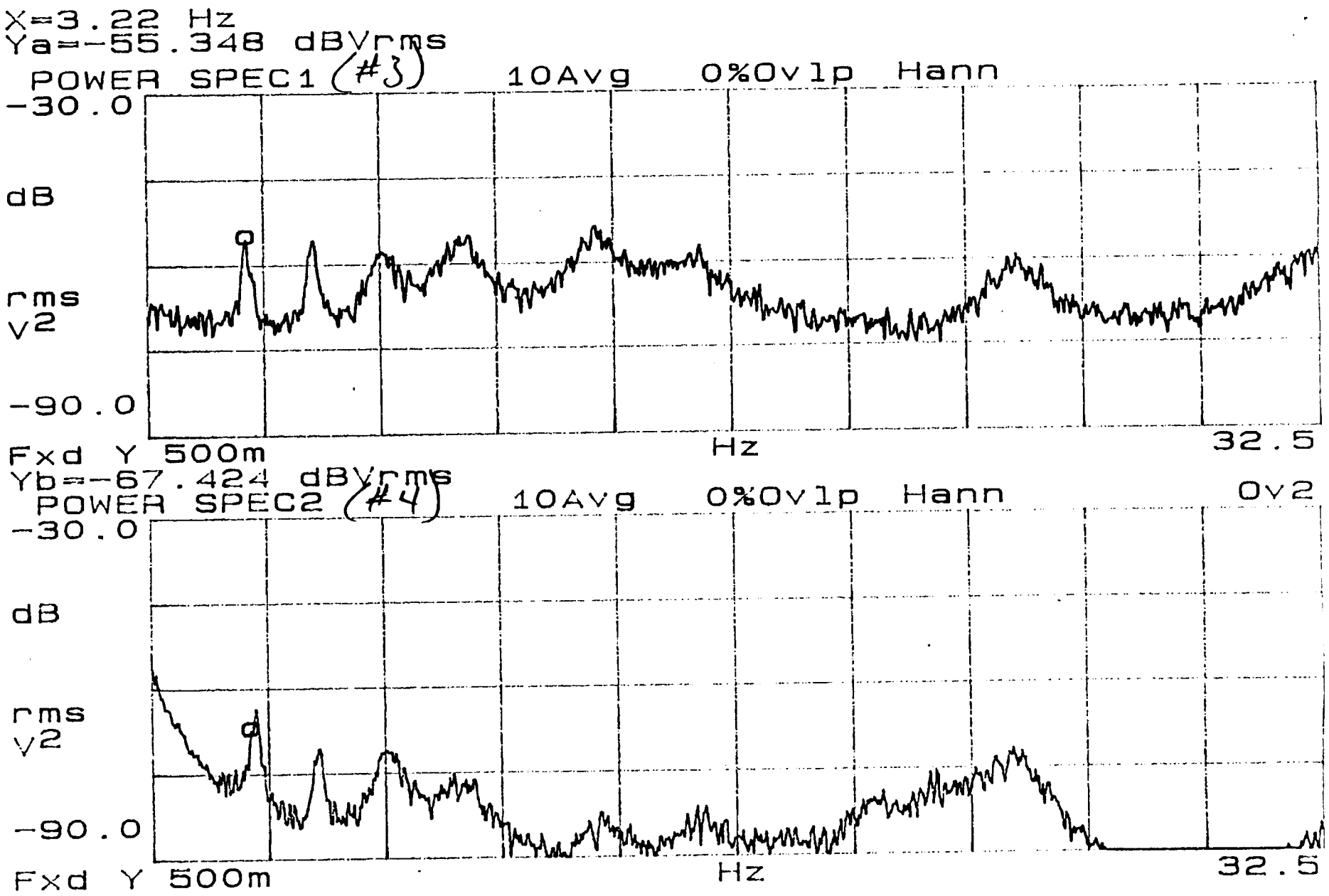

FIGURE 25

6/8/94 $\lambda_M = 0.6$ $\alpha = 0$

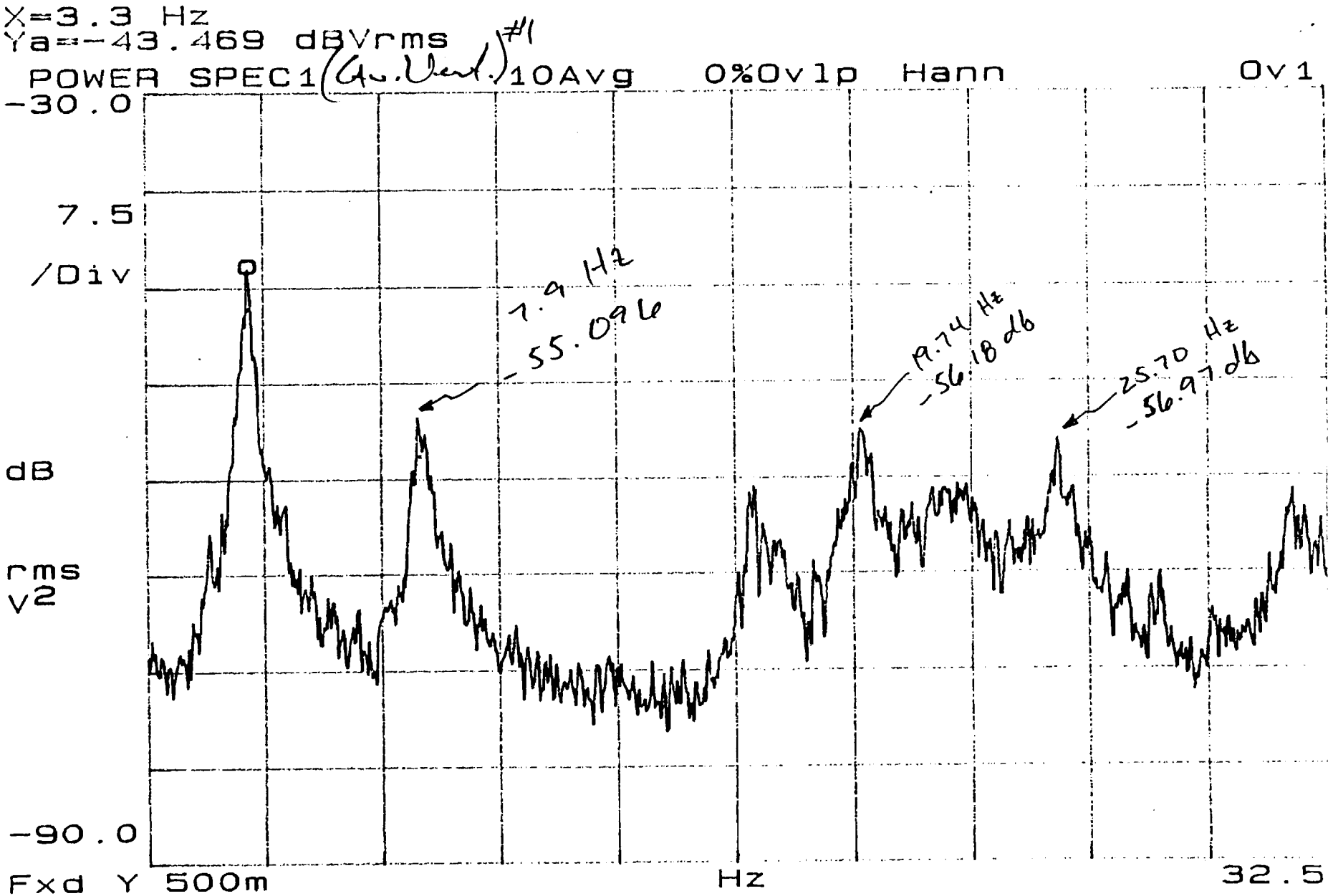

Figure 26

6/8/94 $\lambda_m = 0.6$ $\alpha = 0$

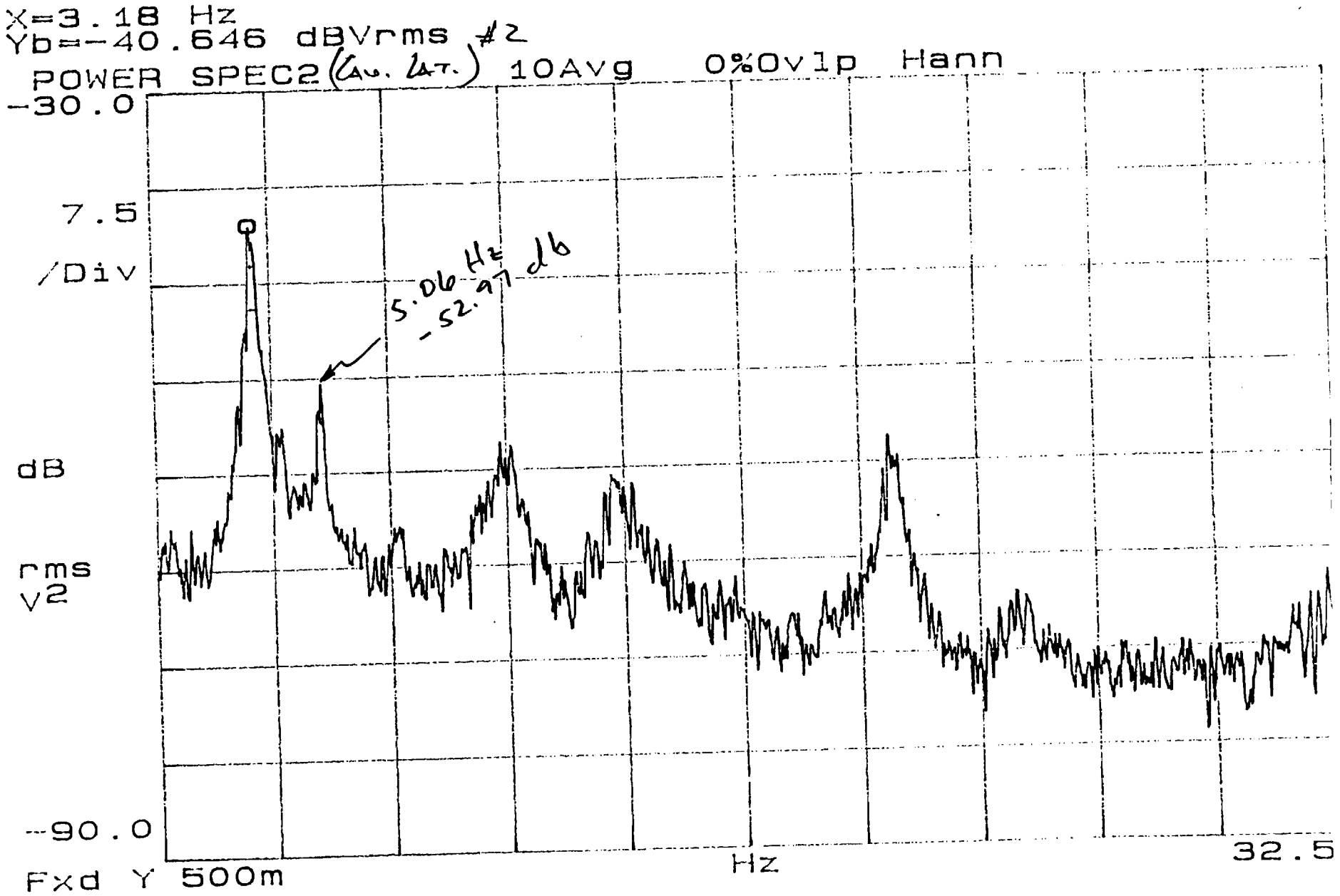

FIGURE 27

6/8/94

$\Omega_M = 0.75 \quad \alpha = 0$

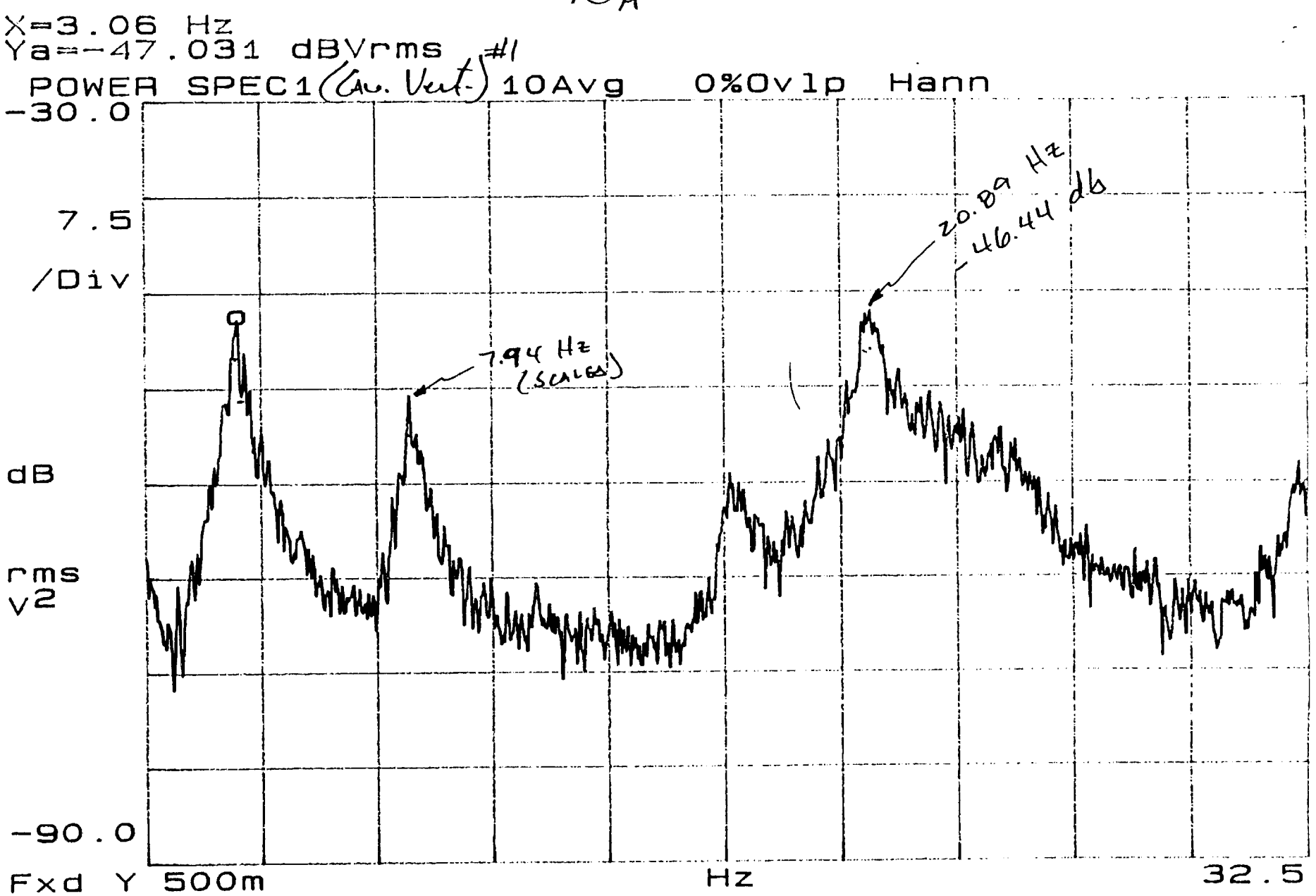

FIGURE 28

6/8/94

$N_M = 0.75 \quad \alpha = 0$

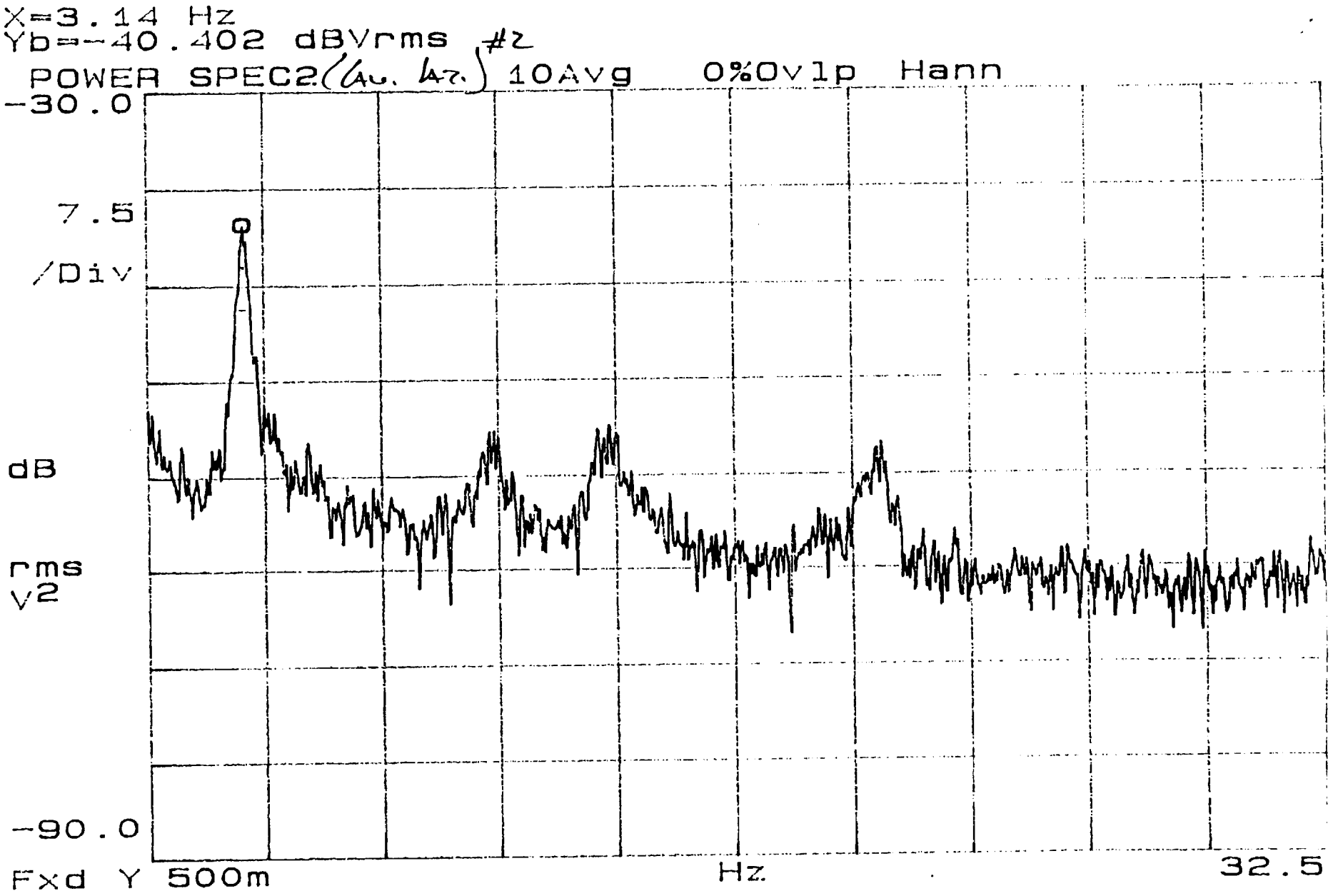

FIGURE 29

NASA Center | ENGINEERING DIVISION | DATE 4/9/94 PAGE ___ of ___

TITLE VERTICAL BENDING MODE
CAV. VERTICAL (#1)

NAME R Sowester CODE ___
CH'KD BY ___ DATE ___

+ ≡ DAMPING ESTIMATE
⊙ ≡ AMPLITUDE

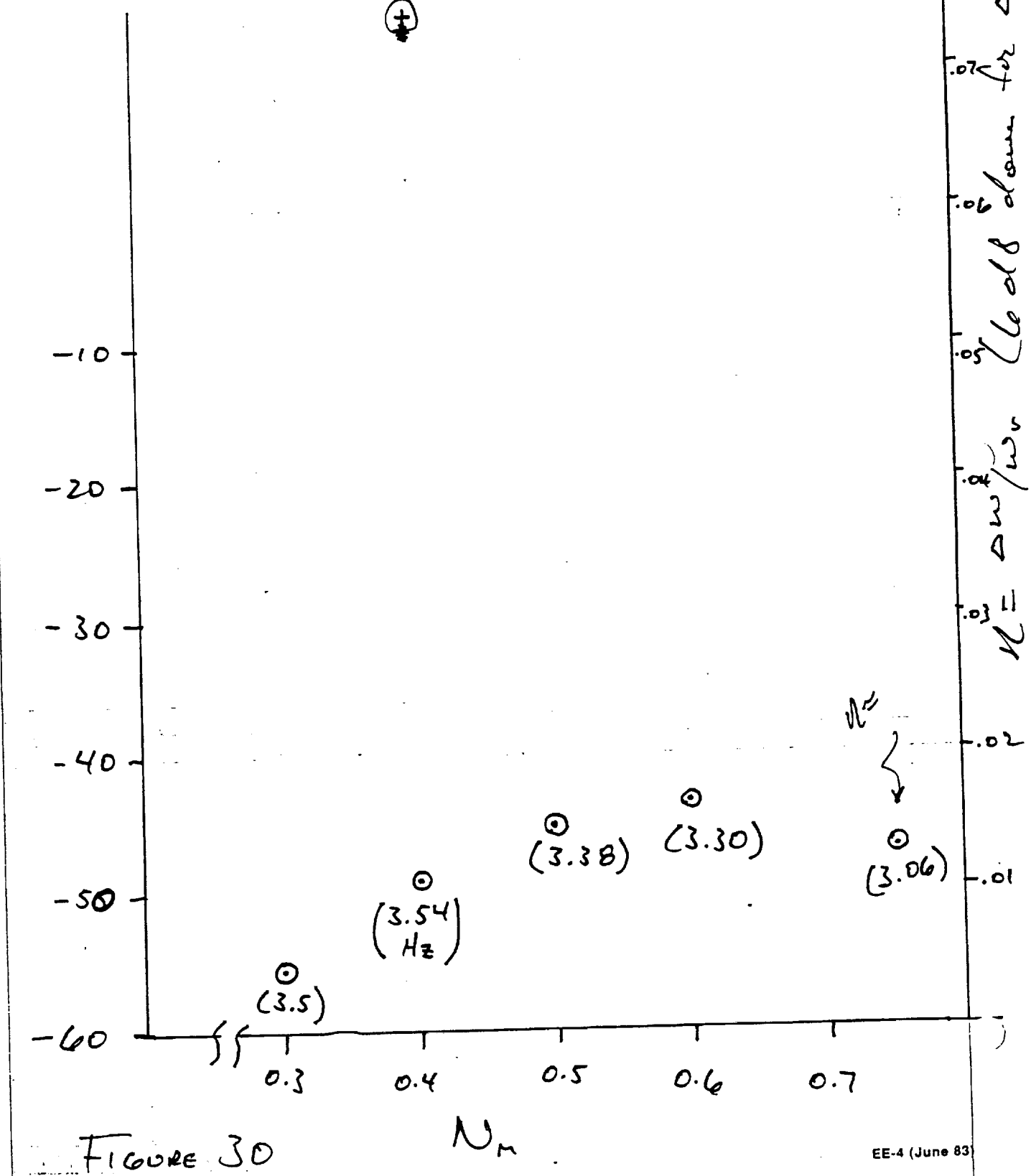

FIGURE 30

EE-4 (June 83)

TITLE Lateral Rocking Mode
Cav. Lateral (#2)

NAME P Spencer CODE ___

CH'KD BY ___ DATE ___

+ ≡ Damping Estimate

⊙ ≡ Amplitude

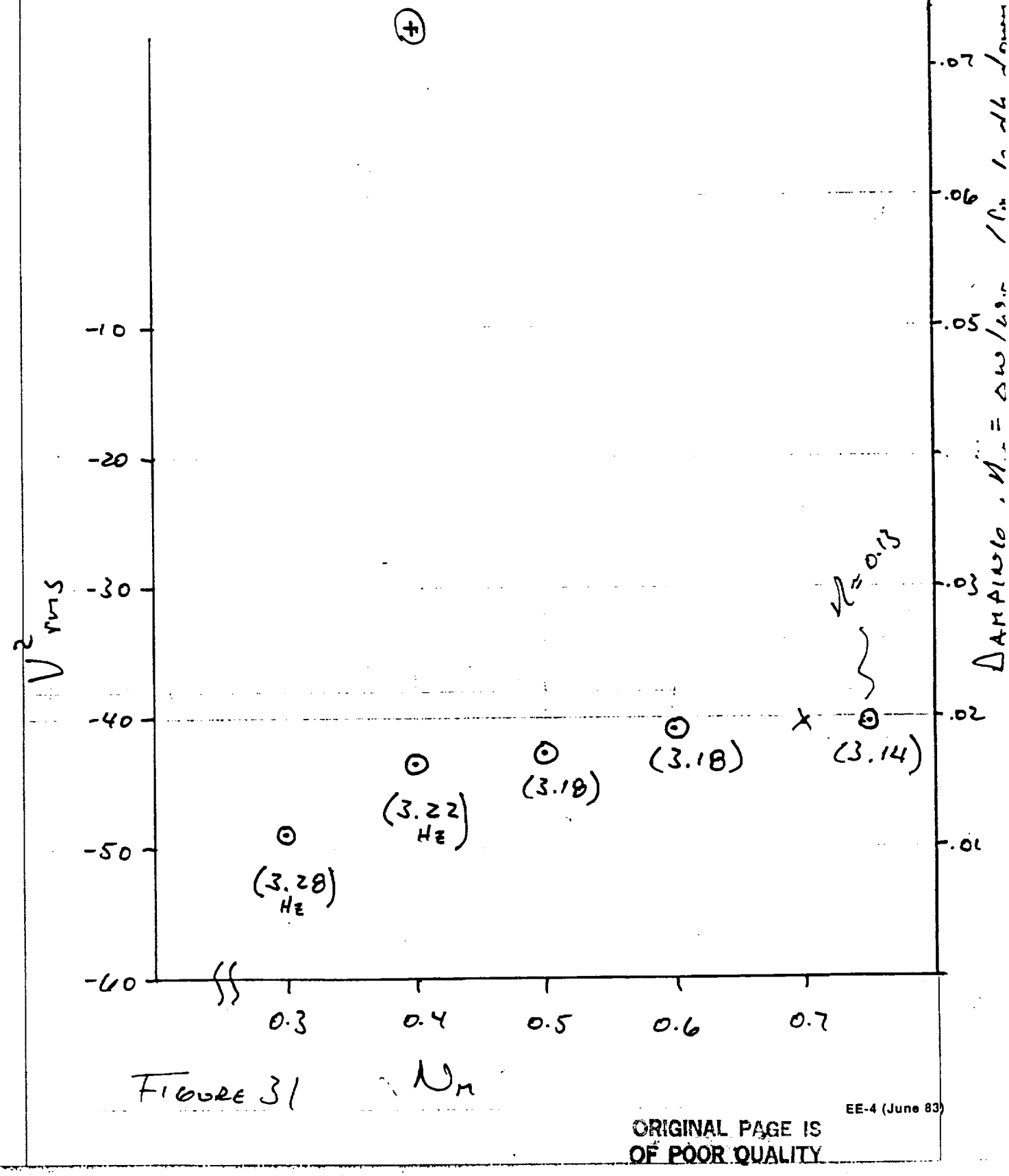

Figure 31

EE-4 (June 83)

NASA Ames Research Center | SYSTEMS ENGINEERING DIVISION | DOCUMENT NO.

DATE 6/10/94 PAGE ___ of ___

NAME P BREWSTER CODE ___

CH'KD BY ___ DATE ___

TITLE TRACKING OF MODE AT 19.54 Hz, NM=0.5 CAVITY VERTICAL (#1)

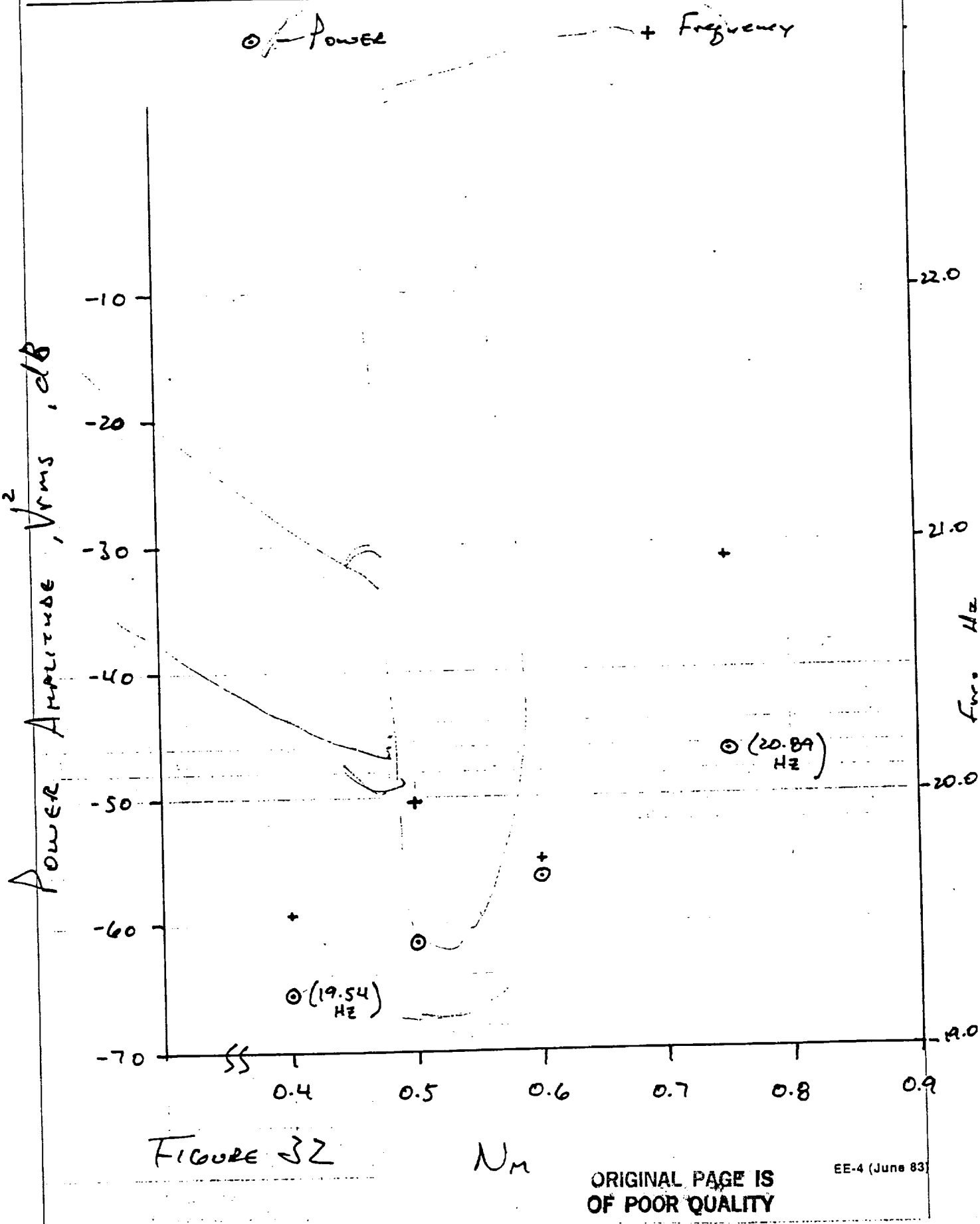

FIGURE 32

EE-4 (June 83)

ORIGINAL PAGE IS OF POOR QUALITY

6/13/94

$N_M = 0.75$

NLC

$\alpha = 0$

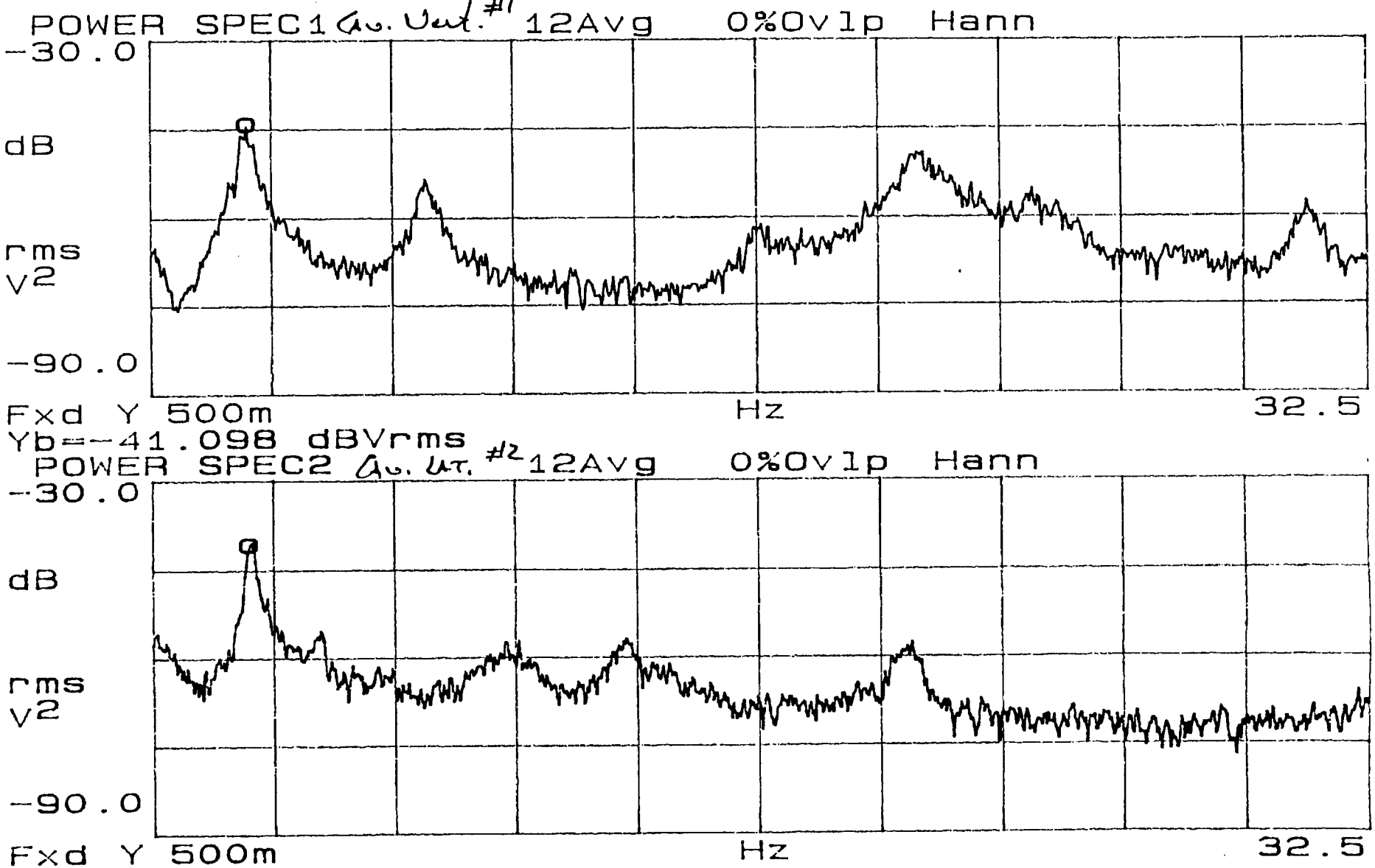

FIGURE 33

6/13/94

$N_M = 0.79$ (No Load Coma)

$\alpha = 0$

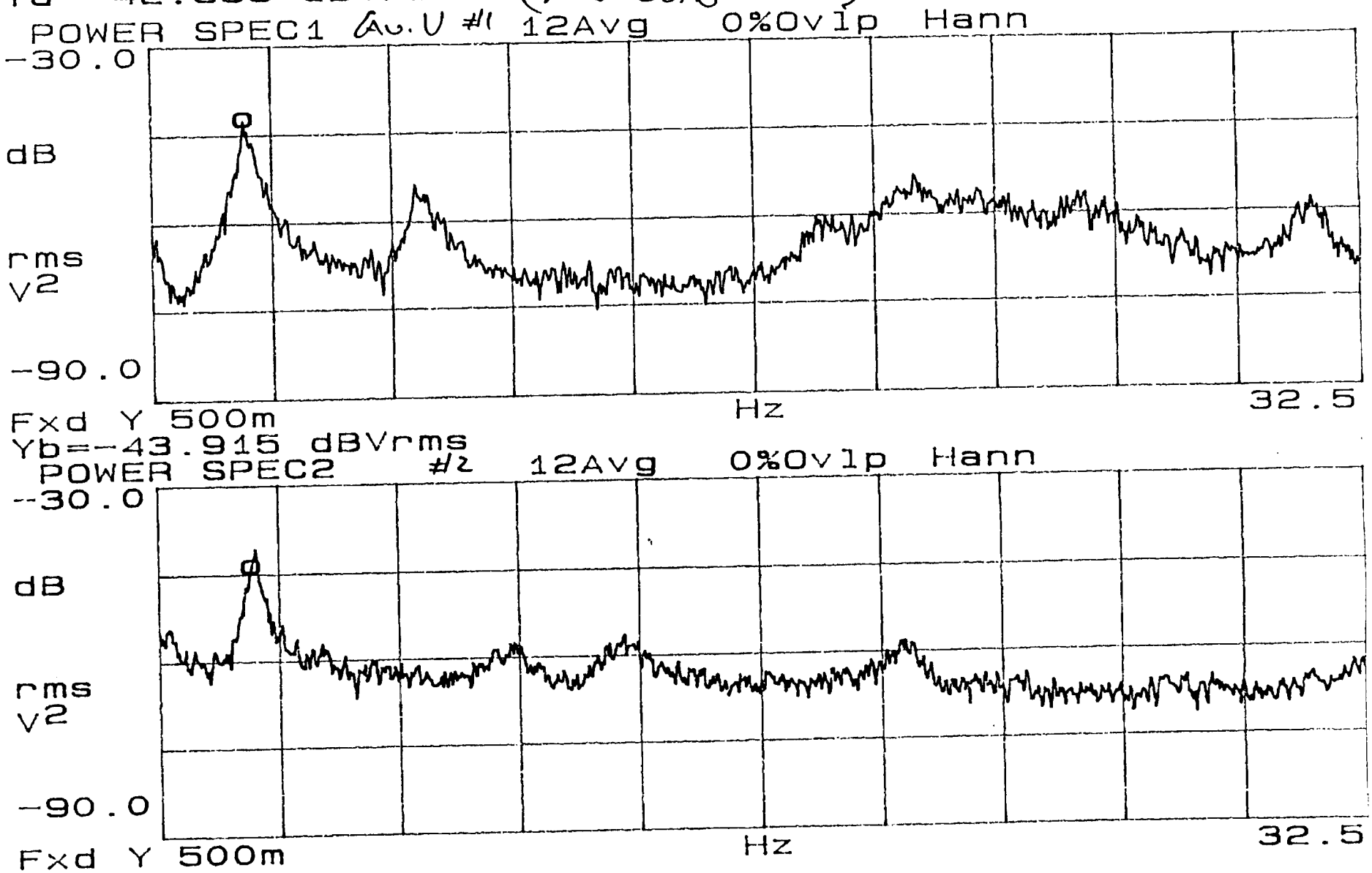

FIGURE 34

6/13/94

$N_R = 0.85$

NLC

$\alpha = 0$

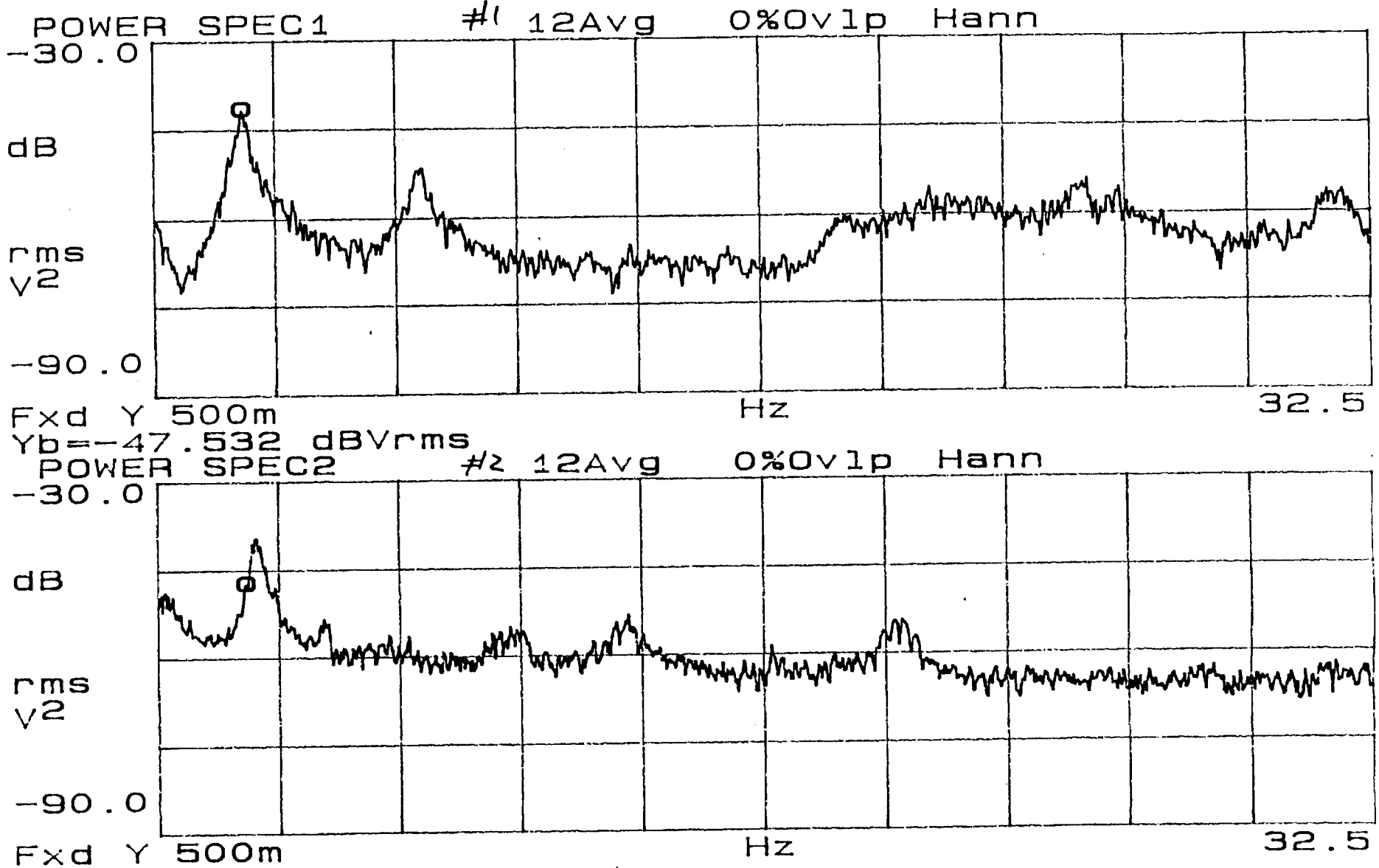

FIGURE 36

6/13/94 $M_\infty = 0.88$ NLC $\alpha = 0$

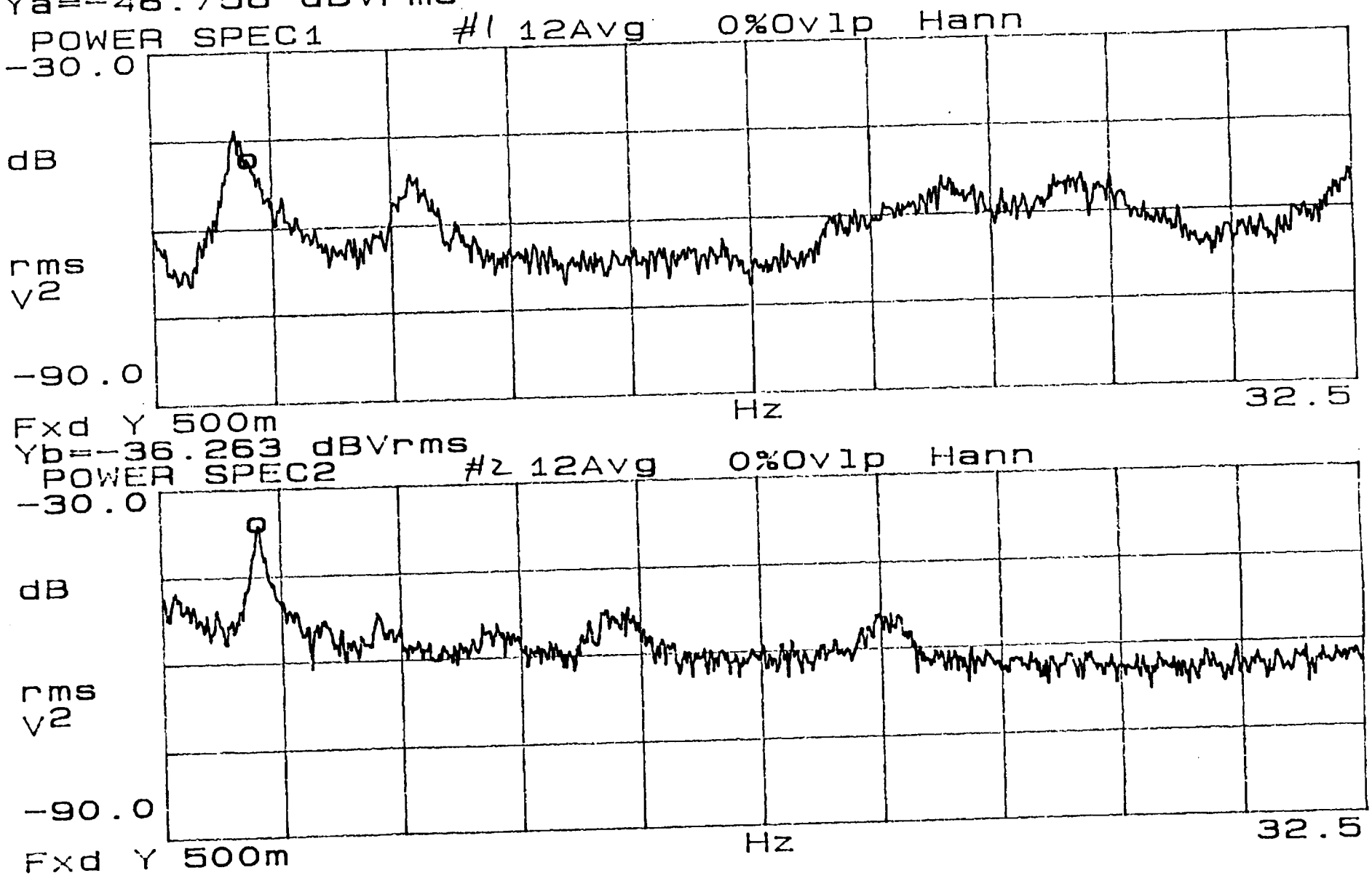

FIGURE 37

6/13/94 $N_M = 0.88$ $\alpha = 0$

X=38.75 Hz
Ya=-70.392 dBVrms (Freq Range = 30 → 230 Hz)

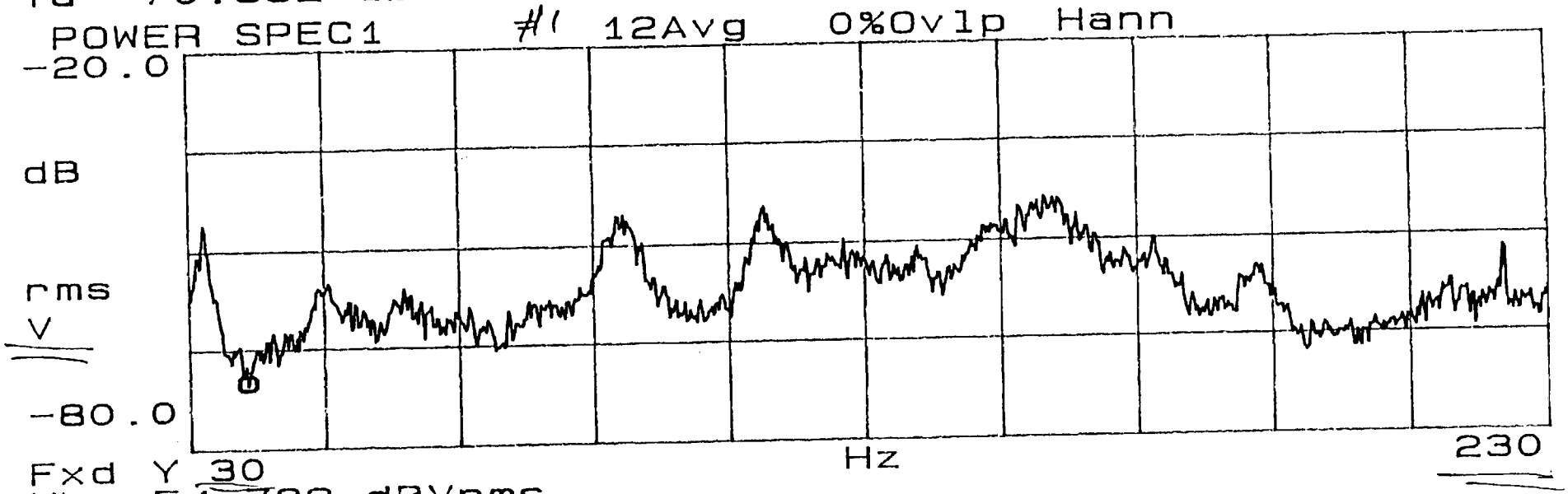

Yb=-54.782 dBVrms

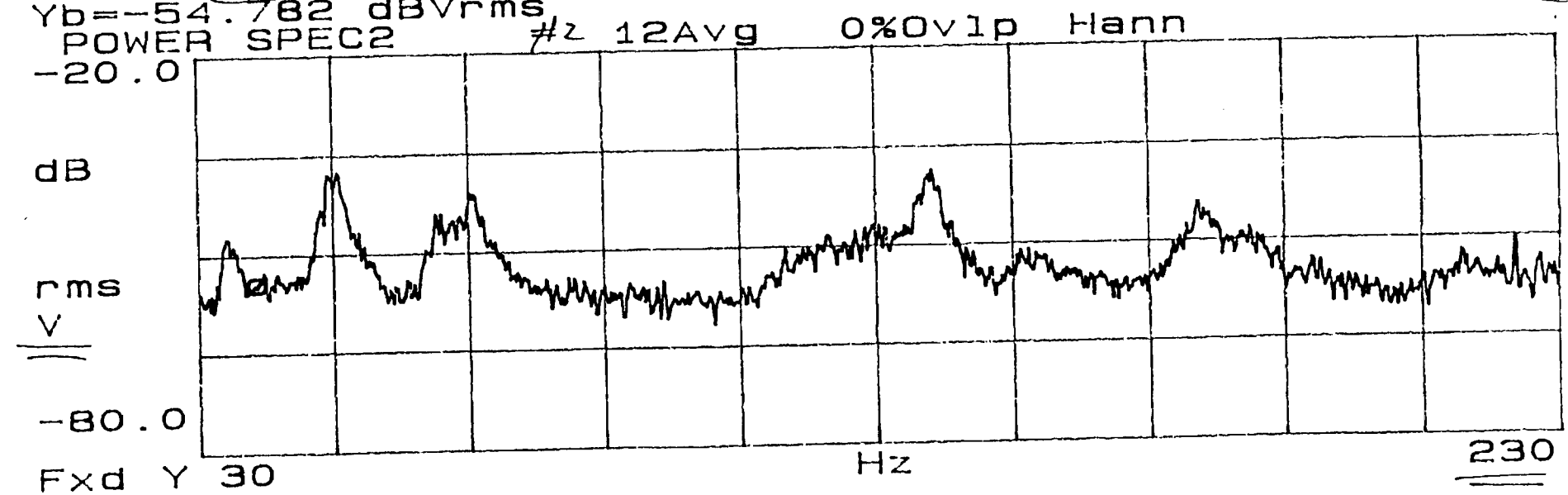

Figure 3B

6/13/94

$\lambda_D = 0.88$

$\alpha = 0°$

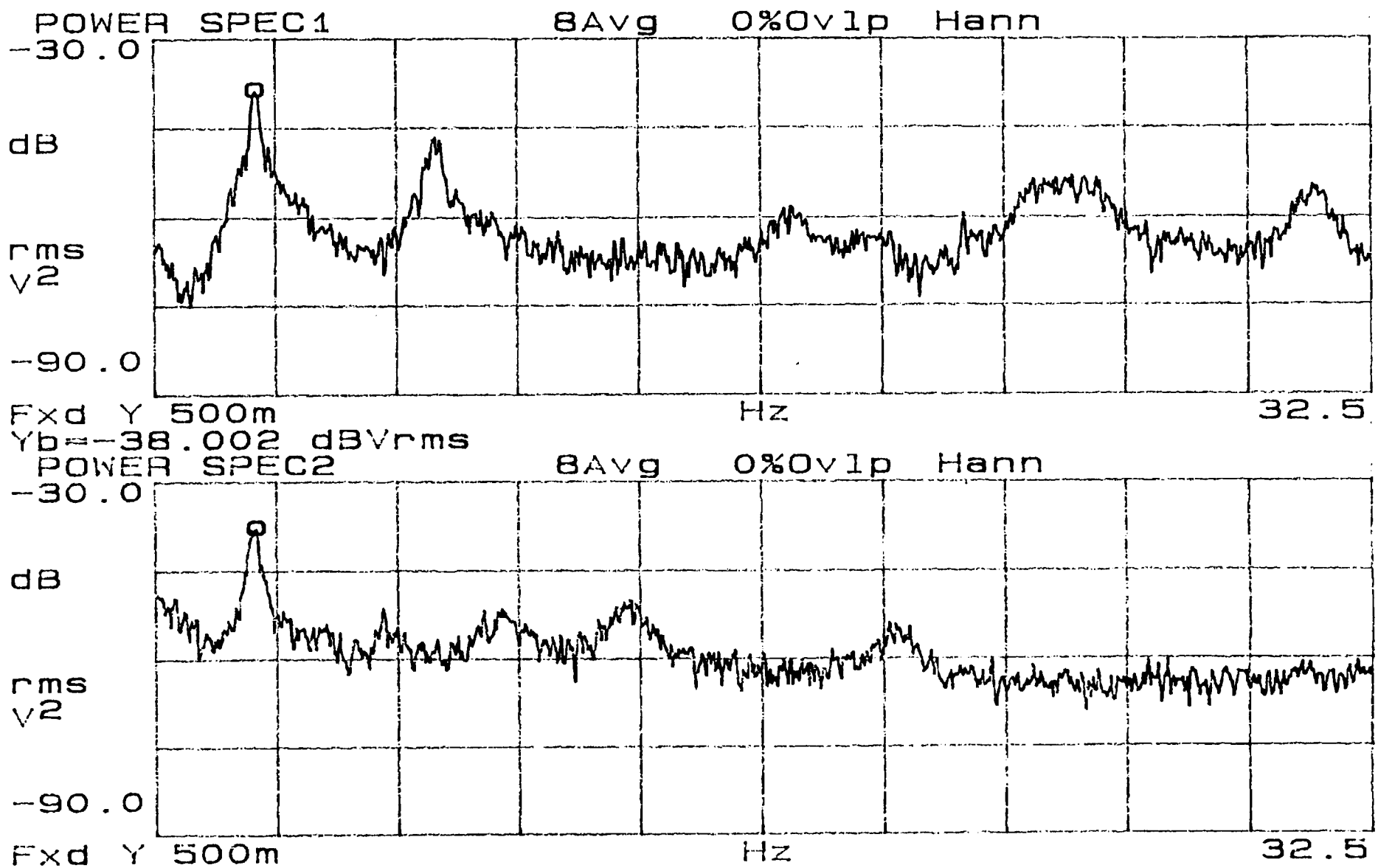

FIGURE 39

6/13/94 $M_n = 0.88$ $\alpha = 1^\circ$

wlc

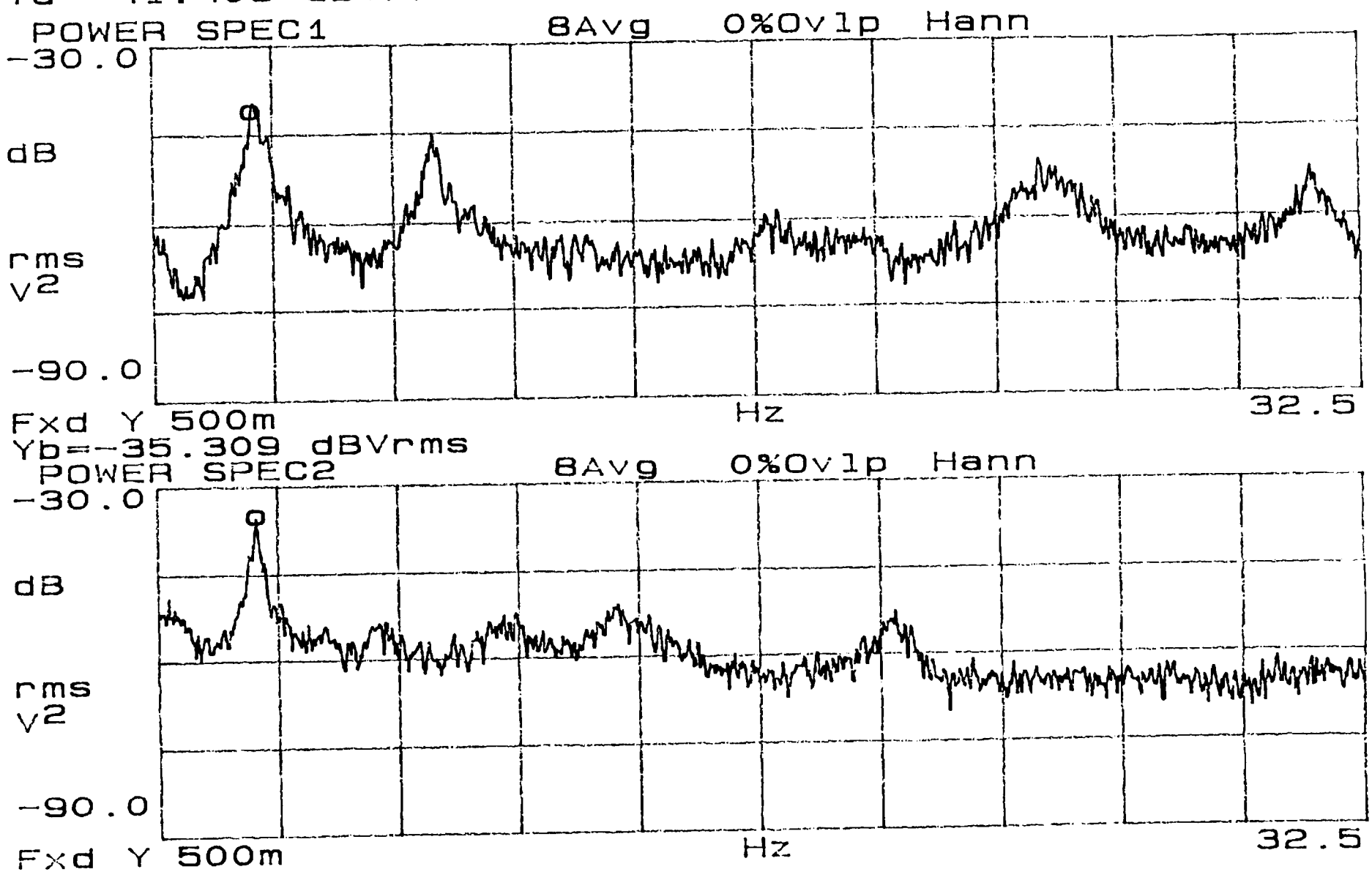

FIGURE 40

6/13/14

$M_\infty = 0.88$

$\alpha = 2°$

wlc

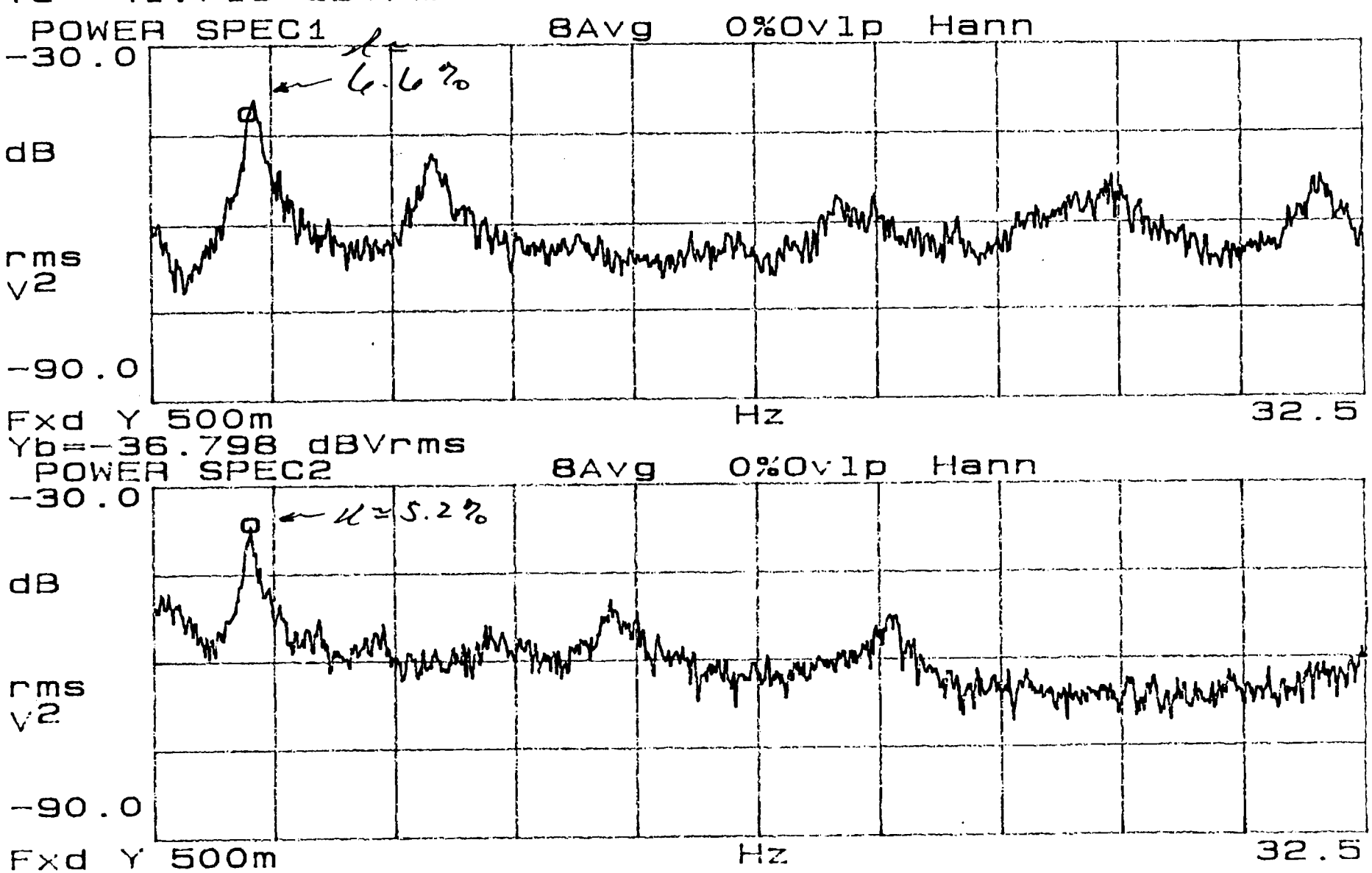

FIGURE 41

6/13/94

$N_M = 0.88$

WLC

$\alpha = 3°$

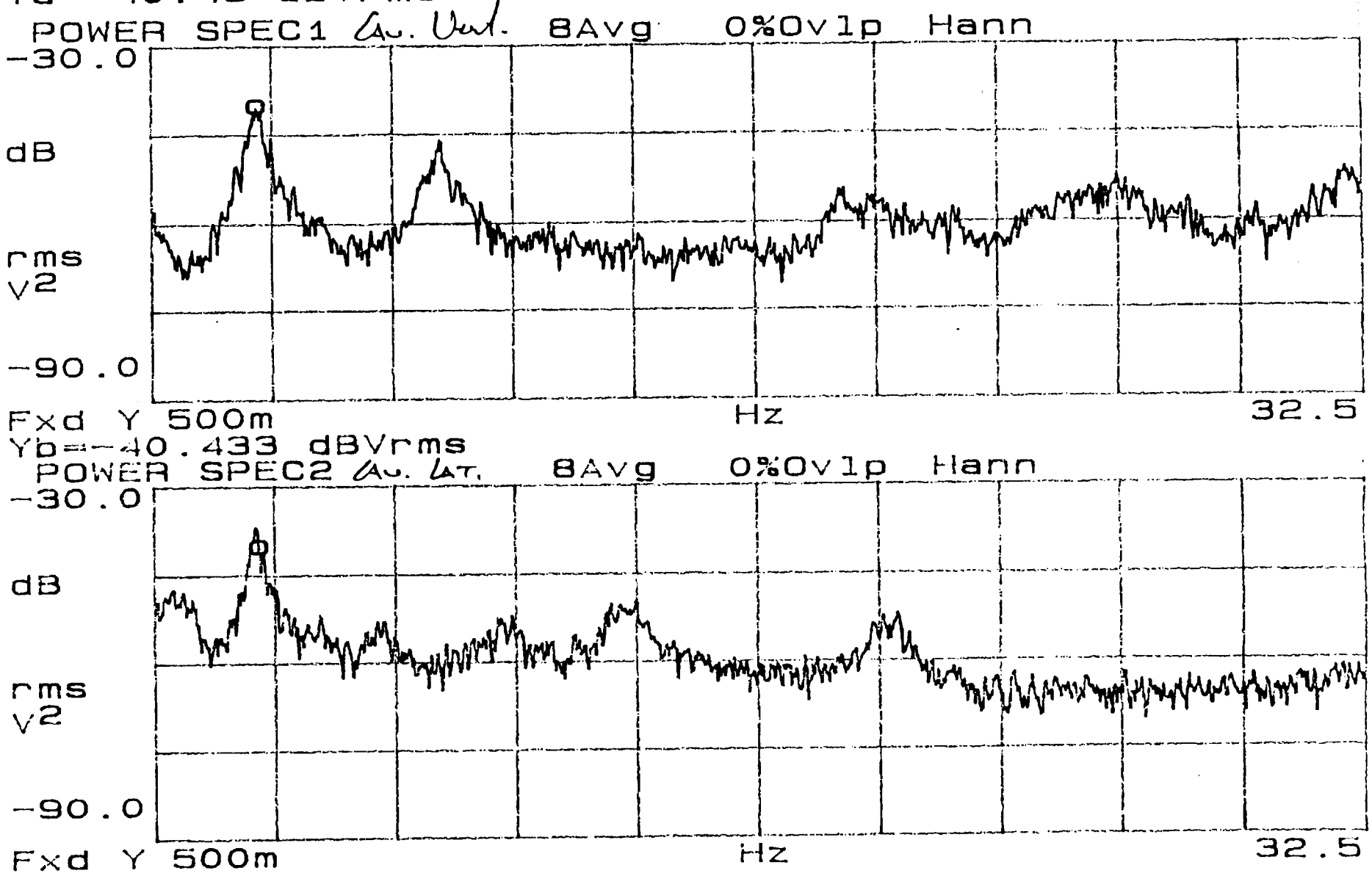

FIGURE 42

6/13/94

$N_m = 0.88$

wlc

$\alpha = 4.0°$

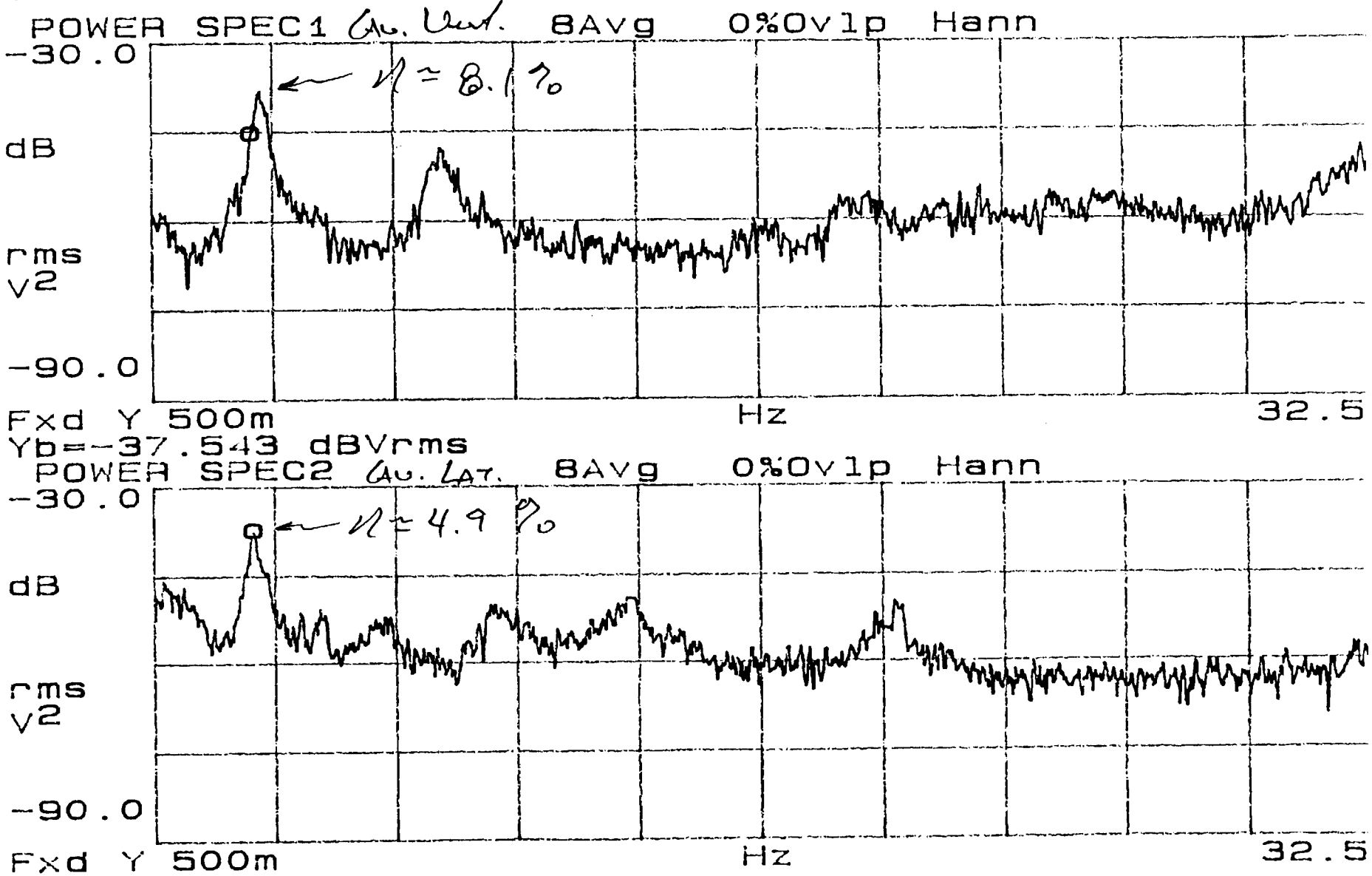

FIGURE 43

6/13/94

$N_n = 0.88$

WLC

$\alpha = 4°$

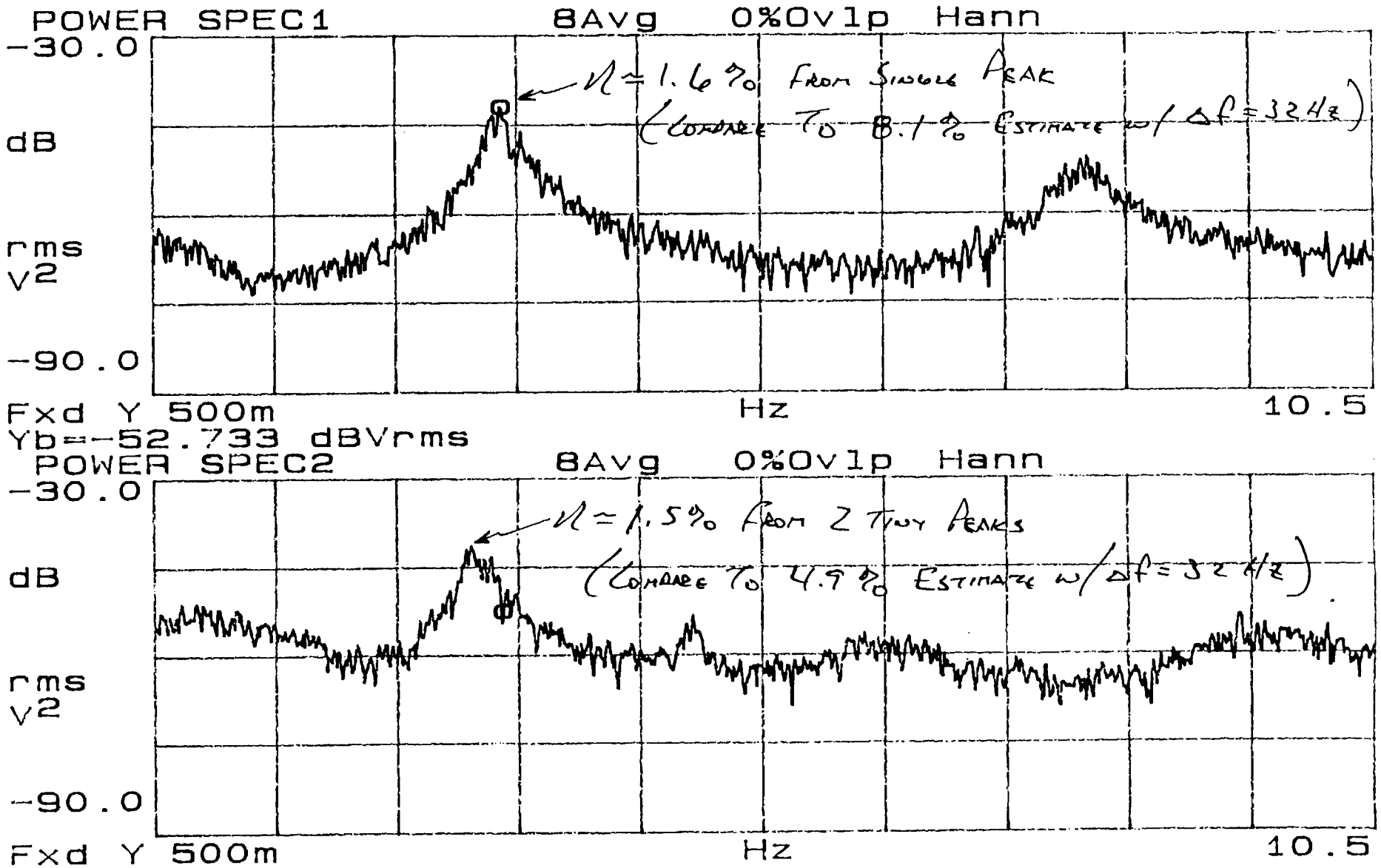

FIGURE 44 (DATA RUN SUBSEQUENT TO SAME N_n & α BUT THE FREQ. RANGE OF 0.5 Hz - 10.5 .8 Hz)

10/13/94

$M_M = 0.88$

$\alpha = 4^\circ$

w LC (Same Data, But Rescaled

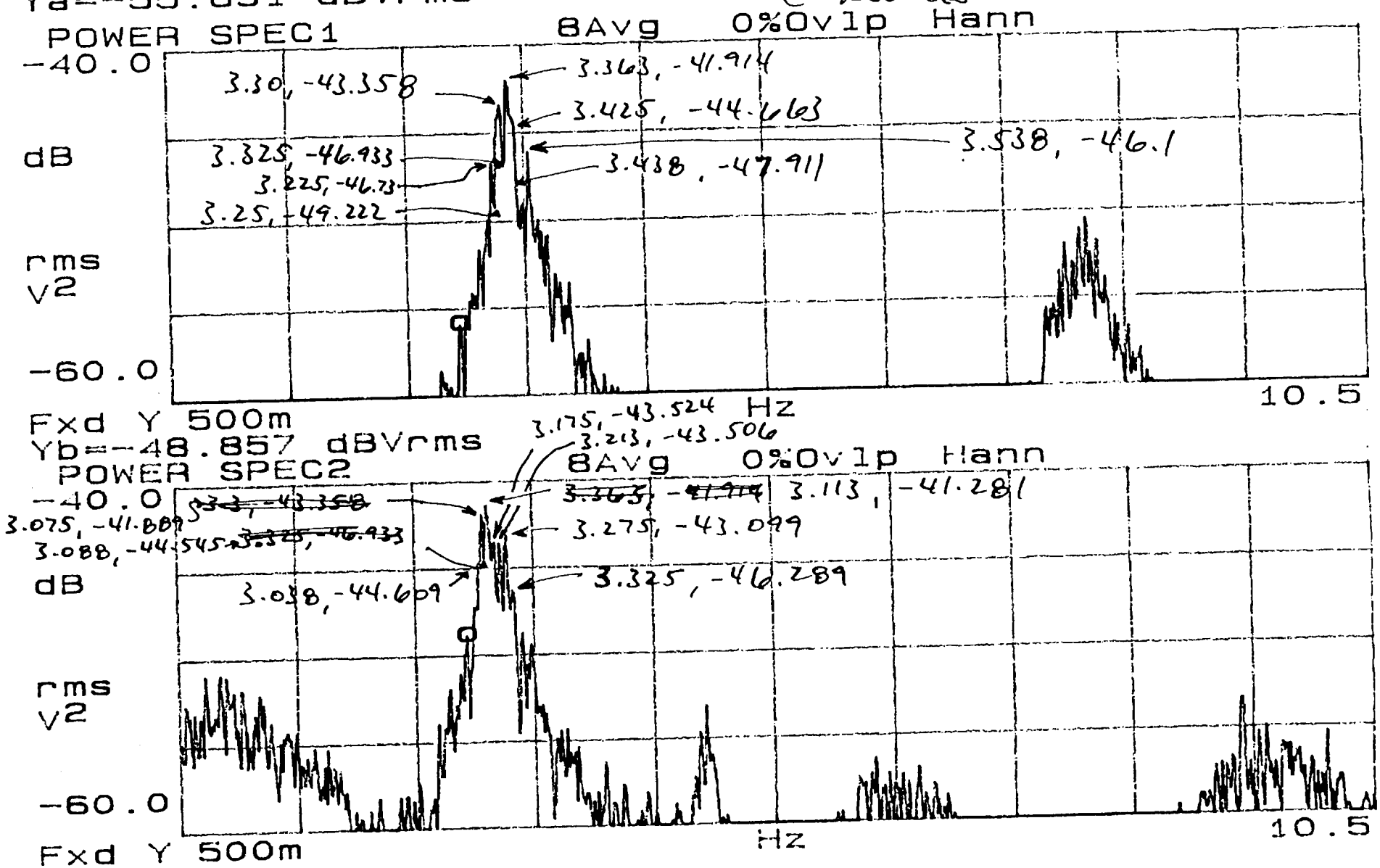

FIGURE 45